Review Paper

Regional scale hydrologic modeling of a karst-dominant geomorphology: The case study of the Island of Crete

Anna Malagò [a,c,*], Dionissios Efstathiou [b], Fayçal Bouraoui [a], Nikolaos P. Nikolaidis [b], Marco Franchini [c], Giovanni Bidoglio [a], Marinos Kritsotakis [d]

[a] European Commission, Joint Research Centre, Institute for Environment and Sustainability, Ispra, VA, Italy
[b] Technical University of Crete, 73100 Chania, Crete, Greece
[c] University of Ferrara, Engineering Department, Ferrara, Italy
[d] Decentralized Administration of Crete, Directorate of Water, 71202 Heraklion, Greece

ARTICLE INFO

SUMMARY

Crete Island (Greece) is a karst dominated region that faces limited water supply and increased seasonal demand, especially during summer for agricultural and touristic uses. In addition, due to the mountainous terrain, interbasin water transfer is very limited. The resulting water imbalance requires a correct quantification of available water resources in view of developing appropriate management plans to face the problem of water shortage.

The aim of this work is the development of a methodology using the SWAT model and a *karst-flow model* (KSWAT, Karst SWAT model) for the quantification of a spatially and temporally explicit hydrologic water balance of karst-dominated geomorphology in order to assess the sustainability of the actual water use. The application was conducted in the Island of Crete using both hard (long time series of streamflow and spring monitoring stations) and soft data (i.e. literature information of individual processes). The KSWAT model estimated the water balance under normal hydrological condition as follows: 6400 Mm³/y of precipitation, of which 40% (2500 Mm³/y) was lost through evapotranspiration, 5% was surface runoff and 55% percolated into the soil contributing to lateral flow (2%), and recharging the shallow (9%) and deep aquifer (44%). The water yield was estimated as 22% of precipitation, of which about half was the contribution from spring discharges (9% of precipitation). The application of the KSWAT model increased our knowledge about water resources availability and distribution in Crete under different hydrologic conditions. The model was able to capture the hydrology of the karst areas allowing a better management and planning of water resources under scarcity.

Contents

---

* Corresponding author at: European Commission, Joint Research Centre, Institute for Environment and Sustainability, Ispra, VA, Italy.
    E-mail address: ing.anna_malago@libero.it (A. Malagò).

1. Introduction

"Karst" identifies a specific geological landscape and morphology formed by the dissolving action of water on soluble carbonate rocks such as primarily limestone, but also marble, dolomite, and gypsum. These rocks are mechanically strong but chemically soluble with high degree of secondary porosity. As a consequence, the hydrological cycle provides the primary source of energy for karst formation because water is the solvent that dissolves carbonate rocks and then carries the ions away in solution (Williams, 2004).

The process of dissolution ('karstification') leads to the development of caves, sinkholes, springs and sinking streams that are typical features of a karst system. With progressing karstification, groundwater flow in the karst aquifer develops from a flow in an interconnected fissure network to a flow concentrated in several large pipes, interconnected cavities and cave systems (EC, 2003, 2004). The downstream end of a karst system usually is a spring where the underground conduit reaches the surface as an output point from an extensive network of groundwater conduits (Smart and Worthington, 2004).

In Europe, soluble carbonate rocks are widespread in Western, Southern and Eastern part covering 35% of whole Europe (Daly et al., 2002), so that the karst processes are significant components of the physical geography of Mediterranean basins. In particular, limestones reach great thickness in Spain, southern France, Italy, the Balkan Peninsula, Turkey and in many islands in the Mediterranean (Crete, Majorca and Sicily). As a consequence, karst aquifers and springs are an important source of water supply for Mediterranean countries and special strategies are required to manage the quantity and quality of their waters.

Bakalowicz (2015) pointed out the importance to study the karst aquifer functioning and the local geological evolution in order to manage in realistic and sustainable way the water resources. The monitoring and management of these resources are recognized in Europe as an essential issue and the European Union prompted the creation of COST Actions 620 and 621 to develop a comprehensive methodology for risk assessment and for the sustainable management of karst systems (EC, 2003, 2004). Unfortunately, most countries are lacking behind in monitoring the discharge of springs or wells and the exploitation of karst aquifers in generally is inappropriate (Bakalowicz, 2015).

In this context, large scale hydrologic models are essential tools for watershed management at regional scale. Regional scale models with an appropriate discretization of watershed can adequately account for the spatial heterogeneity improving water predictions (Wooldridge and Kalma, 2001). A variety of karst models have been developed and applied to karst watersheds (Nikolaidis et al., 2013). Recently, Hartmann et al. (2015) presented for the first time the simulations of groundwater recharge in Europe with a grid-hydrological model (VarKarst-R) pointing out the importance of a characterization of subsurface heterogeneity.

Baffaut and Benson (2009) modified the SWAT (Soil and Water Assessment Tool) model to simulate faster aquifer recharge in a Missouri karst watershed (SWAT-B&B) modifying deep groundwater recharge equations, increasing the hydraulic conductivity of sinkholes simulated as ponds and losses from streams. After that, Yachtao (2009) further modified the SWAT model in order to improve the simulation of water quality and quantity in the Opequon Creek watershed (USA). The author introduced two new parameters for simulating the hydrology and nitrate transport in a sinkhole and losses from sinking streams. More recently, Wang and Brubaker (2014) proposed a non-linear modification of groundwater algorithm in SWAT (ISWAT) improving the recession and low-flow simulation. Nikolaidis et al. (2013) developed a reservoir model approach linked with SWAT to simulate karst's behavior and the recharge of springs of Koiliaris basin in Crete adding five new parameters.

All these studies indicate that a specific parameterization of aquifer discharge, return flow, stream losses and sinkholes is required in karst watersheds. In addition, Wang et al. (2014) showed that a specific database of karst SWAT soils should be used to assess the influence of soil hydrological process in a karst region.

In this paper the SWAT model was integrated with a *karst-flow model* (Nikolaidis et al., 2013; Tzoraki and Nikolaidis, 2007). Karst-subbasins were defined in order to reproduce more accurately the water balance at regional scale.

This integrated model, KSWAT model, was applied to the Island of Crete, one of the most intensively managed Mediterranean islands, where the major water use is irrigation (84.5% of the total consumption) and the main water source is karst aquifers. The growing water demand of the region makes the rational management of water resources extremely important in view of a sustainable development. Consequently, the specific objective of this study is the development of a large scale methodology for the quantification of a spatially explicit water balance of karst-dominated geomorphologies using the SWAT model in order to assess the sustainability of water use in the Island of Crete and potentially to other areas.

2. Materials and methods

2.1. Study area

The Island of Crete occupies the southern part of Greece and is the largest island of Greece and the fifth in the Mediterranean. The Island covers an area of 8336 km^2 and is divided into prefectures, including from east to west: Lasithi (1810 km^2), Heraklion (2626 km^2), Rethymno (1487 km^2) and Chania (2342 km^2) (Fig. 1a). The maximum length of the Island is 269 km and the maximum width 60 km. Four main mountains run west to east: the White Mountains in the west (2453 m), Idis mountain (2456 m) in the center, Asterousian (1280 m) in south Heraklion and Dikti (2148 m) in the east (Baltas and Tzoraki, 2013).
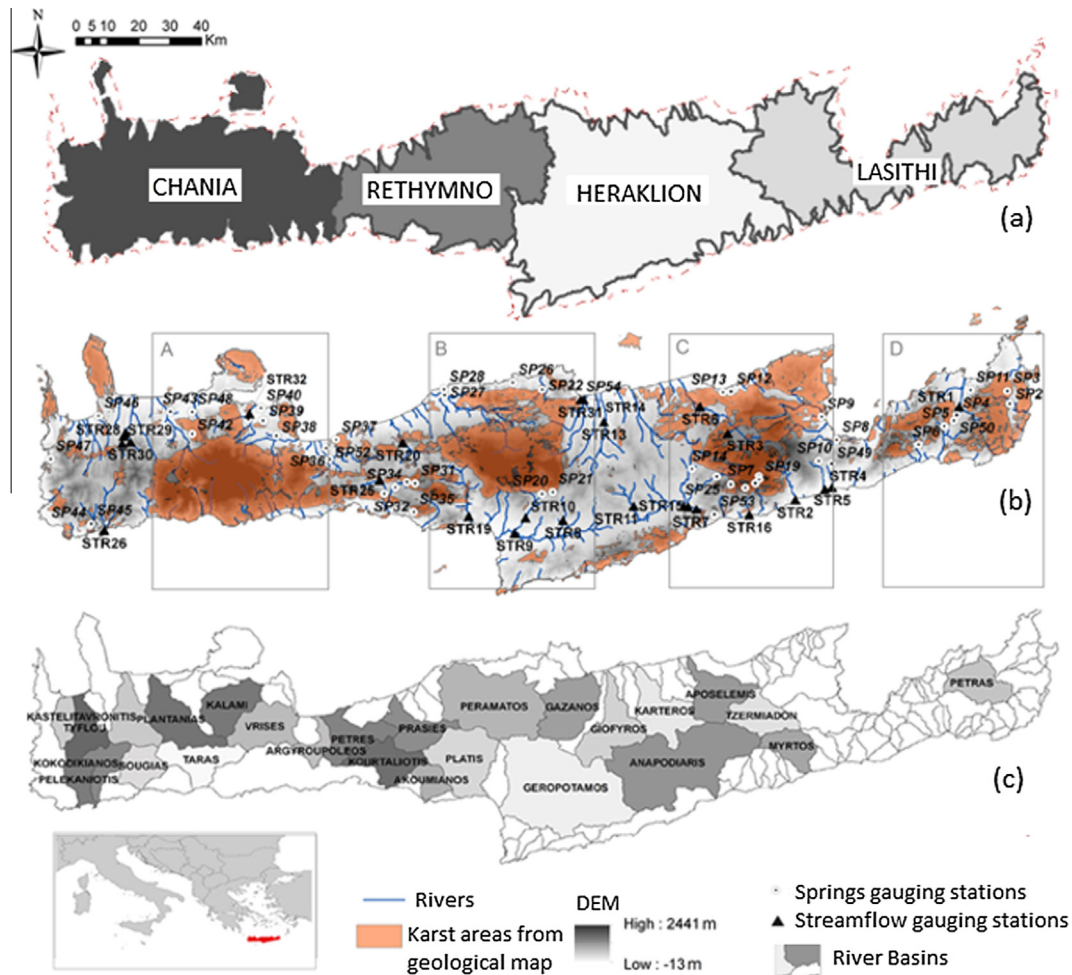
Fig. 1. Map of prefectures (a); the main carbonate rocks of Crete (karst areas from geological map) with springs and streamflow gauging stations (b) A, White Mountainous; B, Idi; C, Dikti; D, Sitia; map of the main river basins (c).

Table 1
Description of available streamflow and spring discharges measurements in the Crete Island provided by the bureau of Water Resources at the Decentralized Administration of the Region of Crete. The symbol # represent the number.

Type of measure	# gauging stations	Type of location	Type of measures	Frequency	Period extension	# Calibrated gauging stations	# Validated gauging stations
Streamflow	22	Permanent gauging station	Water depth	Continuous measurements on a graphic record (Rantz et al., 1982)	1980–2009 (30 years; #5120 data entries)	15	7
Spring Discharge	47	Permanent gauging station	Water velocity	Once a month	1983–2005 (23 years; #8015 data entries)	47	–

The Island of Crete is characterized by a dry semi-humid Mediterranean climate with dry and warm summers and humid and relatively cold winters where mean annual rainfall decreases from west to east and from north to south, but increases with altitude (MEDIWAT, 2013). Annual precipitations are highly variable ranging between 300 mm in coastal areas and 2000 mm in headwaters in White Mountains. The mean annual temperature ranges from 18.5° in the west to 20° in the south of island and decreases with altitude.

The mountainous areas, in particular in the western part, have mountainous climate. As a consequence, Crete contains sub-regions with very different hydrological characteristics.

Crete has about 2550 km² of agriculture land, about 30% of whole Crete, with more than 1100 km² in Heraklion, and 3800 km² of pasture (45% of total areas of Crete). The main crops are olives, grapes, and the main vegetables crops are tomatoes, cucumbers, onions, potatoes, watermelons and melons. The demand for irrigation water is high (about 360 Mm³/y), while only 47% (1200 km²) of agricultural land is irrigated. In Heraklion the irrigated area is around 600 km², followed by Lasithi and Chania with around 300 km², while a very small area in Rethymno is irrigated (Agriculture statistics of Greece, 2005).

2.2. The karst geology and hydrology of Island of Crete

The geology of Crete is composed of carbonate rocks (limestone, marble and dolomite) which allow water to penetrate, creating major karst formation (Baltas and Tzoraki, 2013). More than 30%

of carbonate rocks cover the total area of the Island and the major carbonate rocks of Crete are located in the White mountains (Lefka Ori), Idi, Dikti and Sitia (Fig. 1b). The total karst area covers about 2730 km^2 and the water contribution to the karst aquifer is estimated around 2000 Mm^3/y which discharges out in many springs (Chartzoulakis et al., 2001).

There are 47 gauged springs in Crete with relative large flow, which are subdivided in three main classes: freshwater springs, brackish water springs and undersea springs. Most of springs are karst springs and refer to the same karst hydrogeological system (Lefka Ori, Idi, Dikti and Sitia) discharging around 500 Mm^3/y freshwater into rivers. The most important springs are Stylos, Platanos and Kourtaliotis that discharge 85 Mm^3/y in the Kalami/Koiliaris basin, 67 Mm^3/y in Plantanias Basin and 38 Mm^3/y in Kourtaliotis basin, respectively (Fig. 1c).

Big brackish springs, located on coastal areas, include Almiros-Heraklion that discharges around 235 Mm^3/y, Almiros-Agios-Nikolaos (83 Mm^3/y) and brackish springs of lower discharge include Almiros-Mallia (3.2 Mm^3/y), Georgioupolis, Grammatikaki and Malavra. Brackish springs discharge directly about 285 Mm^3/y in the sea. Submarine discharges can be found in the southern part of Lefka Ori, Souda bay, Bali bay, Mallia bay, Elounta, Skinia, and the eastern part of the limestones of Zakros (MEDIWAT, 2013).

2.3. Streamflow and springs measurements

Stream and spring discharge measurements were provided by the bureau of Water Resources at the Decentralized Administration of the Region of Crete that deals with data elaboration and the assessment of their accuracy. The stream measurements at 25 permanent locations were conducted using a continuous graphic record of the water depth. For a comprehensive description of continuous measurements of water depth, the reader can refer to Rantz et al. (1982).

These measurements were then converted to streamflow rate with an established rating curve (streamflow, m^3/s vs water depth, m) calculated every year for each monitoring station following the procedure described in Buchanan and Somers (1976). The streamflow-water depth relationship was adopted to calculate the streamflow at daily time step, and then aggregated at monthly time step. The available dataset for this study included 22 gauging stations because the streamflow stations STR30 and STR29 were excluded due to their uncertain localization and drain areas. STR5 was also excluded because observed data were lacking during the study period 1980–2009.

The spring's discharges measurements were directly calculated by measuring velocity once a month on surveyed cross-sectional channel geometry at 47 permanent locations. The only exception was the Almiros spring for which only the calculated monthly discharge was available. Table 1 summarizes the streamflow and springs data utilized in this study.

2.4. Approach for the prediction of karst water resources

The proposed karst modeling approach links the process-based model SWAT and a *karst-flow model* (Nikolaidis et al., 2013). Fig. 2 represents the sequential steps of our approach that involved the setup of SWAT model, the identification of karst subbasins in which a modified version of SWAT model was applied, the calibration of streamflow at selected gauging stations (step-wise calibration), the regionalization of calibrated parameters for ungauged subbasins, the spring's discharges calibration outside the SWAT model using the *karst-flow model* and finally the introduction of calibrated discharge of springs as a point sources in the SWAT model. The overall procedure included the use of hard and soft data. Hard data are defined as long-term, measured time series,

typically at a point within a watershed, while soft data are defined as information on individual processes within a budget that may not be directly measured within the study area, generally from literature information (Arnold et al., 2015). In this study long time series of 22 streamflow and 47 of spring monitoring stations were used as hard data, while for instance literature information of the extension of karst recharge areas, as soft data. This approach enables the dialog between local experts, experimentalists and modelers, increases the reliability of the model results in ungauged areas and helps to better constrain model parameters (Seibert and McDonnell, 2002).

2.4.1. The SWAT model

The SWAT model (Arnold et al., 1998) model is a continuous-time, semi-distributed, process based river basin model, originally developed to predict the long-term impact of climate and land use management practices on water, sediment, and agricultural
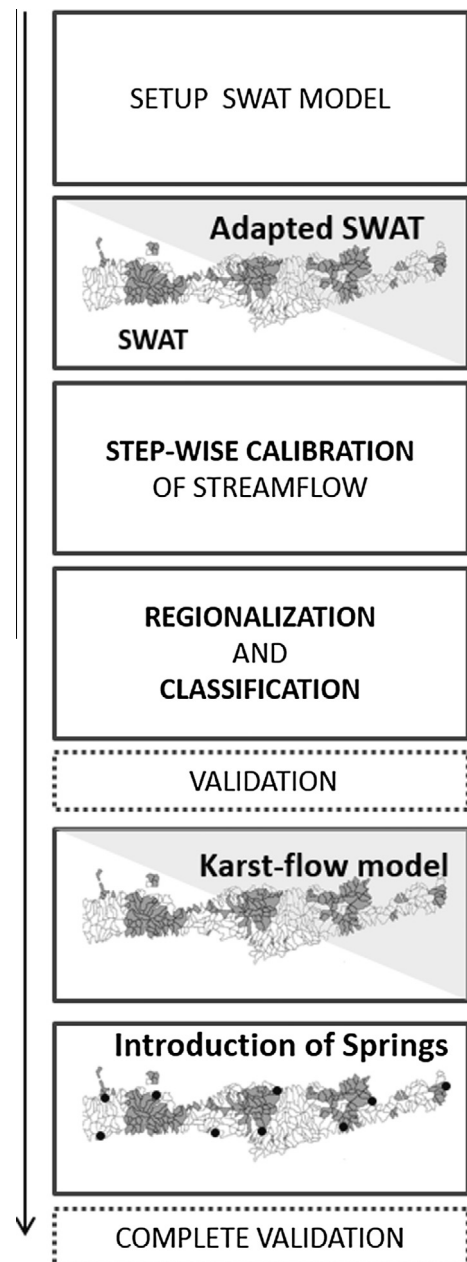

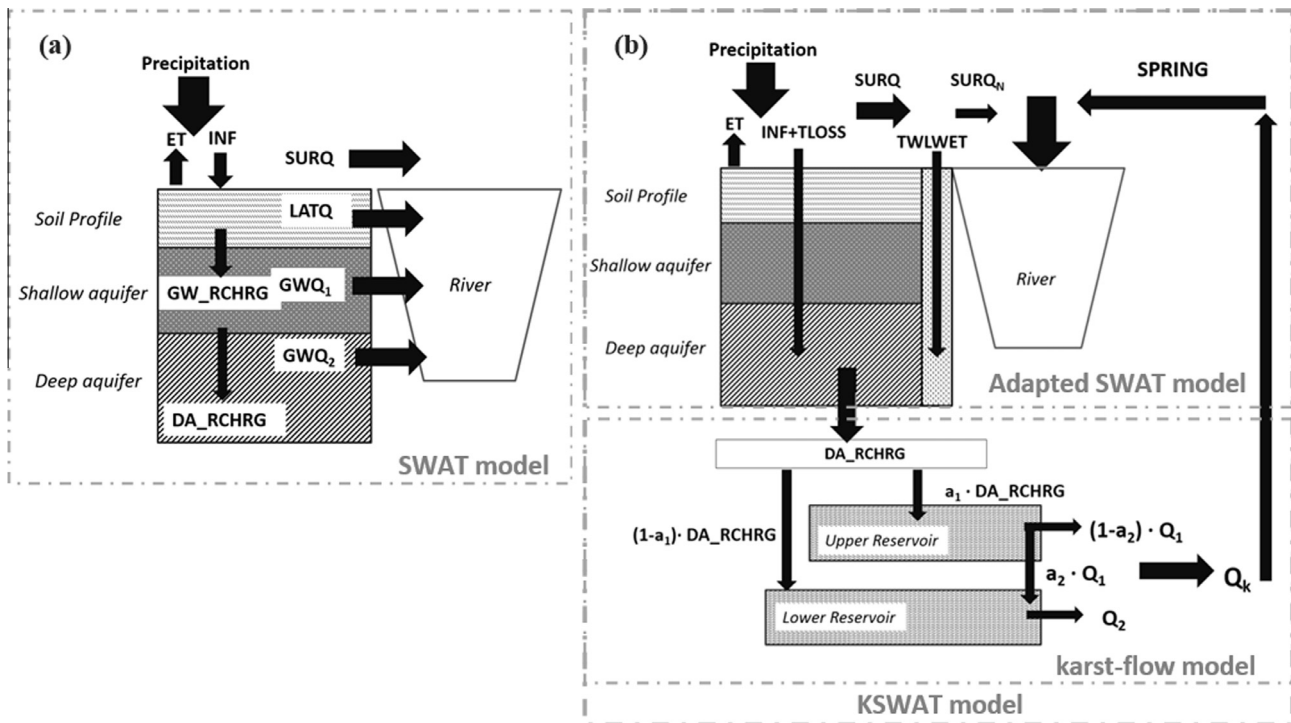**Fig. 2.** Karst SWAT modeling flowchart.

Fig. 3. Comparison between the classic SWAT model configuration and the adapted SWAT model linked with the karst-flow model. In (a): DA_RCHRG, the deep aquifer recharge; ET, evapotranspiration; GW_RCHRG, the shallow aquifer recharge; GWQ_1, baseflow from shallow aquifer; GWQ_2, baseflow from deep aquifer; INF, infiltration in the soil; LATQ, Lateral flow; SURQ, surface runoff. In (b): a_1, fraction of DA_RCHRG to the upper reservoir; a_2, fraction of flow from upper to lower reservoir; DA_RCHRG, amount of direct recharge of deep aquifer from several subbasins (inlet of the karst-flow model); ET, evapotranspiration; INF, infiltration in the soil; Q_1, outlet of upper reservoir; Q_2, outlet of lower reservoir; Q_k, calibrated spring's discharge; SURQ, surface runoff; $SURQ_N$, surface runoff excluding TLOSS and TWLWET; TLOSS, tributary stream losses; TWLWET, losses from the bed of wetlands.

chemical yields in large complex basins. SWAT uses the water balance approach to simulate watershed hydrologic partitioning. In particular, the water balance is calculated considering the snow, soil, shallow aquifer and deep aquifer components.

The watershed is first subdivided into subbasins and each subbasin into hydrologic response units (HRUs) that are a function of soil type, land use and land slope. The main components of the model are: weather, hydrologic mass balance, soil temperature and soil properties, plant growth, nutrients cycling, and sediments yield. SWAT runs on a daily time step. For specific aspects of SWAT, Neitsch et al. (2010) provide a complete description in the theoretical documentation of the model.

2.4.2. Adapting SWAT model to simulate karst processes

SWAT2012 (v.622) uses two linear reservoirs to partition groundwater into two aquifer systems (Fig. 3a): a shallow aquifer which contributes baseflow to streams (GWQ_1) and a deep aquifer which can also contribute baseflow to streams (GWQ_2). The remaining portion in the deep aquifer (DA_RCHRG – GWQ_2) can be considered lost from the system. The recharge for a specific day is calculated as a linear function of the daily seepage, the recharge of the previous day and the groundwater delay. Daily seepage includes seepage through the soil profile, through ponds or wetlands and loosing streams (tributaries and main channels). All seepage losses are added together and assumed to travel vertically to the aquifer with the same velocity. The baseflow from the shallow aquifer GWQ_1 is calculated through the aquifer recharge (GW_RCHRG, mm H_2O), the deep aquifer recharge (DA_RCHRG, mm H_2O) and the baseflow recession constant (ALPHA_BF, 1/day). Similarly, the baseflow from the deep aquifer (GWQ_2) depends on the deep aquifer recharge and on the deep-baseflow recession constant (ALPHA_BF_D, 1/day).

In order to simulate the specific characteristics of karst aquifers (i.e. fast infiltration, movement of water in cave systems) and to calculate the contribution of the karst areas to streamflow as spring flow, the SWAT model structure (Fig. 3a) was adapted as shown in Fig. 3b.

This new SWAT Model structure (Fig. 3b) was the result of the combination of two main studies: Baffaut and Benson (2009) and Nikolaidis et al. (2013) and represents the concept of the karst model and its hydrological pathways. Hereafter, this model configuration is called KSWAT and combines an *adapted SWAT model* and a *karst-flow model*.

In particular, the *adapted SWAT model* considers fast infiltration through caves and sinkholes up to the deep-aquifer, while the *karst-flow model* represents the fast movement of water in subterranean conduits and the lower movement in narrow fractures through the interconnection of reservoirs structure.

The *adapted SWAT model* consists in representing sinkholes by wetlands with small drainage area and a large hydraulic conductivity at the bottom of the wetlands and loosing streams were represented by tributary channels with high hydraulic conductivity in the stream bed.

All the percolation in the soil profile, stream losses and seepage from the bottom of wetlands directly recharges the deep aquifer (DA_RCHRG, mm H_2O). This is achieved by setting the deep aquifer percolation fraction (RCHRG_DP) to 1, imposing minimum groundwater delay (GW_DELAY equal to 1) and setting the groundwater coefficient of capillarity rise ("revap") 0.1 in order to avoid that water moves from shallow into the overlying unsaturated zone while the baseflow from shallow and deep aquifers was imposed negligible (Table 2).

The spring's discharge was simulated with a *karst-flow model* developed in "Excel" environment by Nikolaidis et al. (2013). The

Table 2
Parameters and parameter ranges used in the calibration (in alphabetic order), in the *adapted SWAT model* and in the *karst-flow model*. In column "Process" the information about the order and group of calibration processes: 1, snow process; 2, runoff process; 3, lateral flow process; 4: groundwater process; 5: karst process.

Model	Parameter	Description	Process	Range of calibration values	Range of values in karst-subbasins
Karst-flow model	a_1	Fraction of inflow to upper reservoir	5	0–1	
Karst-flow model	a_2	Fraction of upper reservoir to lower	5	0–1	
SWAT/adapted SWAT model	ALPHA_BF	Baseflow recession constant [1/d]	4/5	0–1	0.1
SWAT	ALPHA_BF_D	Baseflow recession constant for deep aquifer [1/d]	4	0	0
Adapted SWAT model	CH_K (1)	Effective hydraulic conductivity in tributary channel alluvium [mm h^{-1}]	5	–	300
Adapted SWAT model	CH_K (2)	Effective hydraulic conductivity in the main channel [mm h^{-1}]	5	–	5–500 [a]
SWAT	CN2	SCS runoff curve number for moisture condition II	2	−15% to +15%	–
SWAT	EPCO	Plant evaporation compensation factor	3	0.01–1	–
SWAT	ESCO	Soil evaporation compensation factor	3	0.01–1	–
SWAT/Adapted SWAT model	GW_DELAY	Groundwater delay [d]	4/5	0–500	1
SWAT/Adapted SWAT model	GW_REVAP	Groundwater 'revap' coefficient	4/5	0.02–2	0.1
SWAT	GWQMN	Threshold depth of water in the shallow aquifer required for return flow to occur [mm]	4	0–1000	–
Karst-flow model	k_l	Upper reservoir recession constant [1/d]	5	0–5	–
Karst-flow model	k_u	Lower reservoir recession constant [1/d]	5	0–5	–
SWAT	PLAPS	Precipitation laps rate [mm/km]	1	0–100	–
Karst-flow model	Q_{k0}	Initial karstic flow [m^3/day]	5	$0-3 \times 10^5$	–
SWAT/adapted SWAT model	RCHRG_DP	Groundwater recharge to deep aquifer [fr]	4/5	0–1	1
SWAT	REVAPMN	Threshold depth of water in the shallow aquifer for revap to occur [mm]	4	0–500	–
SWAT	SFTMP	Snowfall temperature [°C]	1	−5 to +5	–
SWAT	SMFMN	Minimum melt rate for snow on Dec 21 [mm °C^{-1} d^{-1}]	1	0–10	–
SWAT	SMFMX	Minimum melt rate for snow on Jun 21 [mm °C^{-1} d^{-1}]	1	0–10	–
SWAT	SMTMP	Snow melt base temperature	1	−5 to +5	–
SWAT	SNOEB	Initial snow water content [mm]	1	0	–
SWAT	SOL_AWC	Available water capacity of the soil layer [fr]	3	−25% to +25%	–
SWAT	SOL_K	Saturated hydraulic conductivity [mm h^{-1}]	3	−25% to +25%	–
SWAT	TIMP	Snow pack temperature lag factor	1	0.01–1	–
SWAT	TLAPS	Temperature laps rate [°C/km]	1	−10 to 0	–
Adapted SWAT model	WET_FR	Fraction of subbasin area that drain into wetlands	5	–	0.1–1 [b]
Adapted SWAT model	WET_K	Hydraulic conductivity through bottom of wetland [mm h^{-1}]	5	–	300 [b]
Adapted SWAT model	WET_NSA, WET_MXSA	Surface area of wetlands at normal water level and at maximum water level [ha]	5	–	20 [b]
Adapted SWAT model	WET_NVOL, WET_MXVOL, WET_VOL	Volume of water stored in wetlands when filled to normal, maximum water level and initial volume [10^4 m^3]	5	–	300 [b]

[a] CH-K (2) was manually calibrated in the final calibration.
[b] Wetlands parameters were setting based on geological map extension.

input was the daily deep aquifer recharge (DA_RCHRG, mm) calculated by the SWAT model.

The *karst-flow model* is composed by an upper reservoir with faster response that represents wide conduits in a karst system and a lower reservoir with a slower response that simulates narrow fractures (Kourgialas et al., 2010).

The *karst-flow model* uses the deep aquifer recharge of the surrounding subbasins and involved at the same time the simulation and calibration of springs discharges. The procedure required the contribution/exclusion of deep aquifer recharge of nearest subbasins and the manually adjustment of five parameters of *karst-flow model* minimizing the Normalized Root Mean Square Errors.

These five parameters included: Q_{ko}, the initial karst flow (m^3/day), a_1 the fraction of deep groundwater discharge entering the upper reservoir, a_2 the fraction of flow from the upper reservoir discharge entering the lower reservoir and k_u and k_l were recession constants (1/d) for the upper and lower reservoirs (Table 2). For further details of *karst-flow model* equations, the reader can refer to Nikolaidis et al. (2013) who provided a complete description.

The outputs of the *karst-flow model* were then introduced in SWAT as point sources with aggregated values at monthly time step.

This modified SWAT was applied only in the karst-subbasins identified by three dominant soils that were strongly correlated to the karst areas of the Geological Map (Fig. 4b and c). According to the European Soil Database these are Leptosols (European Soil Portal, 2014), poorly developed and shallow soils over hard rock and comprise of very gravelly or highly calcareous material.

However, the use of the "dominant karst soils" sometimes was limiting since in some cases the size of the subbasins (about 20 km^2) and the fragmentation of soils inside the subbasin did not allow identifying it as "karst subbasin". This occurred for instance in the south-central part of the Island in Kourtaliotis Basin (corresponding to Kourtaliotis river basin in Fig. 1c), where this limitation was overcome using literature information (i.e. Steiakakis et al., 2011) and the geological map. Thus, both karst-soils extension and the geological map were used to identify the karst-subbasins where the KSWAT model was applied. It is
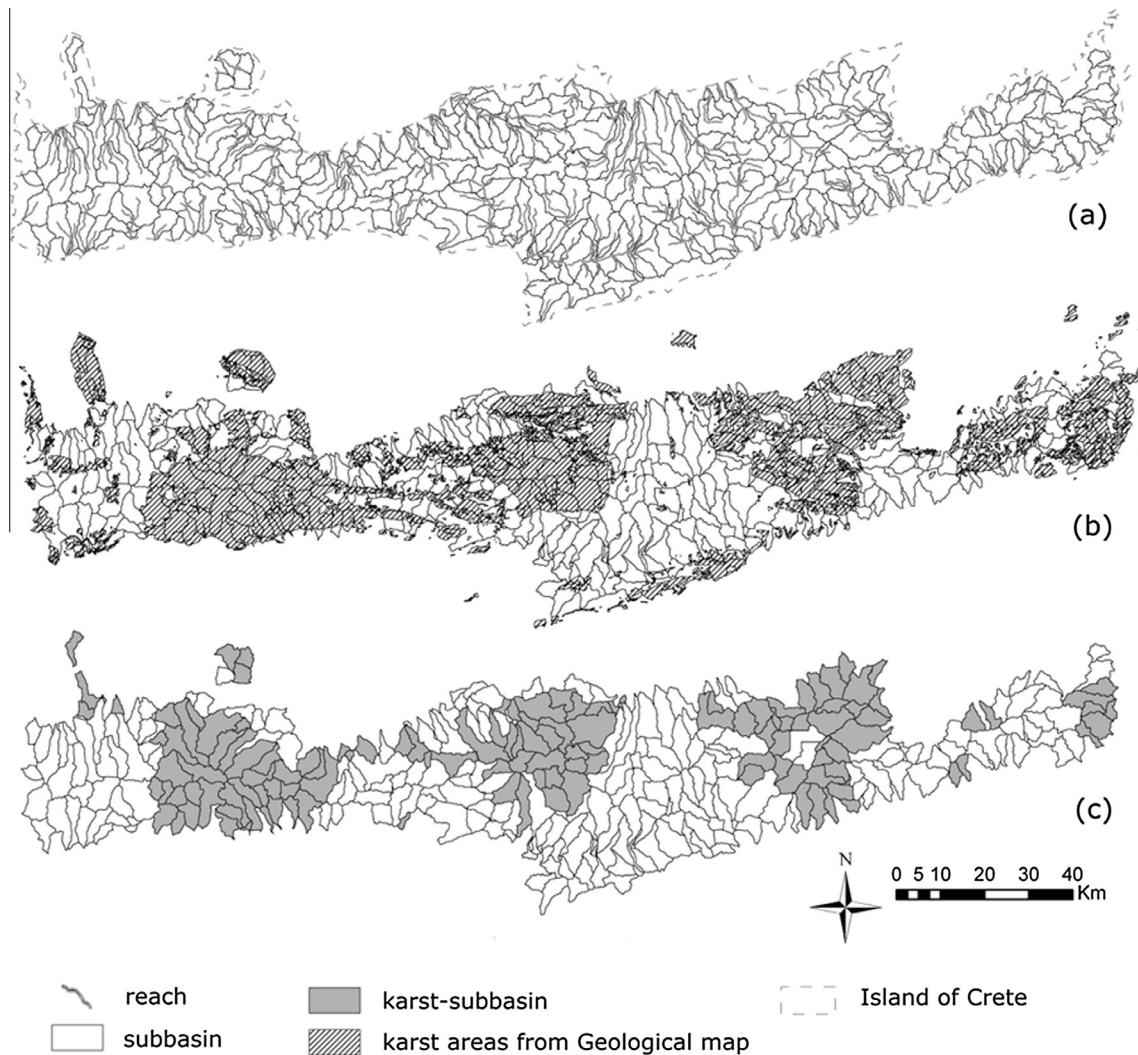
Fig. 4. Rivers and subbasins (a); definition of karst geological features: karst areas from geological map (b) and the subbasins with karst soils (karst subbasins) (c).

noteworthy that the extension of wetlands inside each karst-subbasin was defined using the geological map, generally covering the entire subbasins where the karst-soils are dominant, or only a percentage of subbasin area as in the case of the Kourtaliotis Basin. The resulted area covered by the karst-subbasins was estimated around 2600 km^2.

2.4.3. Model setup

The SWAT model requires pedological, climatological, topographical and land use data. Subbasins were delineated using the ArcSWAT interface with a Digital Elevation Model of 25 m pixel size (EU-DEM; Bashfield and Keim, 2011). The Digital Elevation Map was obtained from a Pan-European elevation data at 1 arc-second (EU-DEM). Subbasins and streams were defined using a drainage area threshold of 1000 ha resulting in 352 subbasins with an average area of 19 km^2 covering 6700 km^2 (Fig. 4a).

Land cover was derived from a 1 km raster map built from the combination of CAPRI (Britz, 2004), SAGE (Monfreda et al., 2008), HYDE 3 (Klein and van Drecht, 2006) and GLC (Bartholome and Belward, 2005) for the year 2005. Land use was obtained from the Agriculture statistics of Greece (2005). For each subbasin the "dominant land cover approach" was used in order to reduce the complexity and the computational level of the model. Six classes of dominant land cover were defined: arable land, pasture,

forest, urban area, water and range grasses. Each subbasin with dominant arable land cover was further subdivided in three parts (15–35–50% of subbasin area) in order to distribute more accurately the crops reported by the Agricultural census. Soil type and characteristics were defined using a 1 km soil raster map, obtained from the Harmonized World Soil Database (HWSD) (FAO, 2008).

From the combination of land use, dominant soils, and single slope for each subbasin the final configuration resulted in 502 HRUs (Hydrological Response Units) with an average area of 13 km^2. The management practices for each crop included planting, fertilization, irrigation and harvesting. The simulated timing of plant sowing and harvesting were implemented in SWAT through daily heat unit concept. In this study the heat units for each crop were calculated by Bouraoui and Aloe (2007) using the PHU (Potential Heat Units) program (PHU, 2007), developed at Texas Agricultural Experiment Station. The PHU program calculates the total number of heat units required to bring a crop to maturity. For each crop the crop growing season (winter versus spring crop), the base growing temperature (°C), the optimum growing temperature (°C), the dry down fraction, the time to maturity (number of days between planting and harvesting) were considered as input in the PHU program. These attributes were related to the different European climatic zone.

The amount of manure and mineral fertilization applied were retrieved from the Common Agricultural Policy Regionalized Impact (CAPRI) agro-economic model (Britz and Witzke, 2008). It provided at NUTS 2 administrative level (Nomenclature of Territorial Units for Statistics) the mineral and organic nitrogen and phosphorus fertilizer application estimated from sectoral statistics and animal production levels.

A manual irrigation was applied selecting the irrigated HRUs for a total irrigated area around 25,000 ha in Chania, 9300 ha in Rethymno, 60,000 ha in Heraklion and 26,000 ha in Lasithi. The total abstractions for irrigation use in each Prefecture was 89 Mm^3/y in Chania, 35 Mm^3/y in Rethymno, 170 Mm^3/y in Heraklion and 66 Mm^3/y in Lasithi, respectively. Both irrigated areas and volumes were obtained from the Agriculture statistics of Greece (2005).

According to the National statistics, the sources of abstraction for irrigation uses were set from deep aquifer and shallow aquifer, and from springs. In the model the abstraction for irrigation from springs (38 Mm^3/y) was implemented as outside-watershed source in the schedule management plan and the corresponding abstractions were subtracted from the daily deep aquifer recharge (DA_RCHRG, m^3/s) (outside SWAT), so that the calibration of springs discharge in the karst-flow model was performed using the net of the abstractions.

The abstractions for drinking water, industry and olive mills (40 Mm^3/y) were introduced in SWAT by subtracting water from the deep aquifer and shallow aquifer at monthly time step, while the abstractions for drinking water from the springs (24 Mm^3/y) were subtracted from the daily deep aquifer recharge (DA_RCHRG) (outside SWAT).

The climate data used in this study include 69 stations with daily data for precipitation and 21 stations for temperature from 1961 to 2009. Monthly statistics of solar radiation, wind speed and relative humidity were calculated using the pan European high-resolution gridded daily data set EFAS-METEO, acronym of European Flood Awareness System – METEO (Ntegeka et al., 2012) for 29 stations uniformly distributed over the modeled territory.

The subbasins were split into elevation bands, and snow cover and snowmelt were simulated separately for each elevation band. In this study steep subbasins were subdivided into 4 classes of elevation.

2.4.4. Calibration of streamflow

For the calibration and validation of the Crete SWAT model 22 stations of streamflow were used. Based on the simplest test technique (Klemeš, 1986), 15 of them were used for calibration and 7 for validation covering the period 1980–2009. The selected subbasins for calibration were headwaters and were uniformly distributed in the Island. The streamflow was calibrated in the 15 selected subbasins in different steps ("step-wise calibration") according to the involved hydrological process, providing a calibrated parameter set NOP (Near Optimal Parameters set). The obtained NOP set was then transposed in ungauged subbasins using the "hydrological similarity approach".

The step-wise calibration is a procedure that allowed calibrating the different components of the streamflow according to different hydrologic processes underpinning each calibration objective. This procedure proposed by Pagliero et al. (2015) and Malagò et al. (2015) was performed using the SWAT-CUP (SWAT Calibration Uncertainty Procedures) programs and the SUFI-2 algorithm (Abbaspour, 2008).

The calibration period covered 30 years from 1980 to 2009 with 10 years of warm up. Among several parameters in SWAT, 19 parameters (see parameters that refer to SWAT and SWAT/Adapted SWAT model in Table 2) were chosen for the streamflow calibration

as the most sensitive and representative of each hydrological process involved in the calibration. The parameters and their initial ranges (Table 2) were selected based on preliminary model runs, literature reviews (van Griensven at al., 2006) and sensitivity test. It is noteworthy however that the parameters in karst-subbasins were not changed keeping the settings of the adapted SWAT model configuration as described in Table 2.

In this work, since the streamflow data was only available at monthly resolution, the streamflow was not divided into the main components (surface runoff, lateral flow, baseflow). However, the calibration was still performed step wise:

Step 1: Calibration of total monthly flow in order to control the timing of runoff signal by adjusting the snow parameters by minimizing the coefficient of determination r^2;

Step 2: Calibration of total monthly flow using only the parameters that regulate the surface runoff process by minimizing the coefficient of determination r^2;

Step 3: Calibration of total monthly flow using only the parameters that regulate the lateral flow process by minimizing the coefficient of determination r^2;

Step 4: Calibration of total monthly flow using only the parameters that regulate the baseflow process by minimizing the Nash Sutcliffe Efficiency, NSE (Nash and Sutcliffe, 1970);

Step 5: Final step, calibration of total monthly flow using all previous parameters together with a reduced uncertainty ranges by minimizing the NSE coefficient.

The coefficient of determination r^2 (Taylor, 1990) was adopted as objective function for the first three steps and the NSE coefficient (Nash and Sutcliffe, 1970) was selected for the fourth and final step as described below. The selection of the objective functions is the result of several tests since the differences between objective functions on parameter sets could be quite striking (Abbaspour et al., 2015). The calibration was performed using 1000 simulation runs at each step.

2.4.5. The regionalization and classification of ungauged subbasins

The Final Near Optimal Parameter set (NOP) of calibrated subbasins (called "donors") was transposed to ungauged subbasins using the hydrological similarity approach. The measure of hydrologic similarity between subbasins is translated into subbasin characteristics which are common for gauged and ungauged watersheds. These characteristics that linked the subbasin characteristics with the hydrological responses have been performed in the literature (Shamir et al., 2005; Oudin et al., 2010). However, for a comprehensive enlightenment of hydrological similarity approach the reader can refer to Wagener et al. (2007) and Sawicz et al. (2011). The calibration for the parameters of the karst-subbasins were kept unchanged using the settings of the adapted SWAT model.

The hydrological similarity approach was performed using the PLSR (Partial Least Squares Regression) that allowed identifying similar subbasins based on the correlation between the watershed characteristics and the discharge characteristics. Following Malagò et al. (2015), this correlation was performed using 17 gauged independent basins using the R package "pls" (Mevic and Wehrens, 2007). The gauging stations selected to perform the PLSR analysis involved stations from the group selected for the calibration and some from the validation group in order to identify a group of stations with almost 8 years of continuous data from 1988 to 1995 that allowed calculating robust statistical indices.

For the selected subbasins 20 independent variables representing the subbasin characteristics ("c" matrix) and 2 dependent flow variables ("q" matrix) were used in the PLSR analysis as the

responses and regressors (q ~ c) (Malagò et al., 2015). The independent variables included river length (km), minimum, maximum and average elevation (m), median slope (%), content of clay and sand in the soil, percentage of different classes of land cover (%), percentage of karst area, mean annual precipitation (mm), minimum, maximum and average temperature (°C), annual potential evapotranspiration (mm) and average number of days with precipitation. The dependent variables included the mean annual discharge (mm/y) and the corresponding coefficient of variation. The PLSR analysis defined latent variables that were used to perform the classification of subbasins.

Due to the limited number of potential donors (15 subbasins, 4% of total number of subbasins), it was necessary to define "hydrological regions" and then the "classification" of similar subbasins was performed inside each region. For a review of regionalization techniques, the reader can refer to Parajka et al. (2005).

Using the latent variables, the regionalization was performed with the Ward's hierarchical cluster analysis (Ward, 1963) based on the Euclidean distances and the classification of subbasins in donor's classes was pursued inside each hydrological region according to the K-Nearest-Neighbor using the R package "supclust" (Dettling and Maechler, 2012). The classification of each sub-

Table 3

Comparison of observed and simulated streamflow in the period 1983–2009 after the introduction of the springs (complete validation): in the first two columns the code and name of the stations; in the third column the drain area (km^2); the % data represents the % of observed monthly values in the period 1983–2009 (324 total months); the observed and simulated volumes are respectively Mm^3/year OBS and SIM; the performance indicators between monthly observed and simulated steamflow are the normalized root mean square error (NRMSE%), the percent bias (PBIAS%), the Nash Sutcliffe Coefficient (NSE), the coefficient of determination (r^2) and the coefficient of determination multiplied by the slope of the regression line between simulated and observed values (br^2).

Station	Name	Drain area (km^2)	% data	Mm^3/year OBS	Mm^3/year SIM	NRMSE%	PBIAS%	NSE	r^2	br^2
STR32	Koiliaris	132.6	21	180.97	182.74	16.5	3.3	0.68	0.69	0.62
STR19[R]	Platis	209.6	69	50.15	46.30	11.1	2.4	0.63	0.63	0.47
STR7[R]	AnapodiarisH	522.7	54	30.13	31.55	6.9	16.5	0.78	0.8	0.73
STR13	Giofiros	186.3	69	22.24	22.94	12.5	25.4	0.53	0.66	0.65
STR20	Prasanos	101.9	54	17.83	22.17	13.2	2.8	0.23	0.36	0.27
STR9[R]	Geropotamos	394.5	69	17.21	33.04	32.2	183.4	−3.94	0.46	0.24
STR3	Katavothres	21.35	54	16.63	11.56	11	−32.7	0.53	0.62	0.3
STR26	Kakodikianos	78.11	77	15.89	19.02	11.6	31.6	−0.87	0.25	0.23
STR27	Sebreniotis	28.48	80	15.83	12.45	8.5	−17.9	0.58	0.6	0.38
STR11	Anapodiaris Pla	89.51	47	11.89	12.91	13.4	−2	0.64	0.65	0.53
STR10	Koutsoulidis	132.2	54	11.53	13.07	5.7	17.2	0.83	0.84	0.82
STR2[R]	Mirtos	96.34	84	10.87	11.31	15.3	39.9	−0.35	0.29	0.26
STR6[R]	Aposelemis	204.8	69	10.69	26.46	14.4	158.7	−0.05	0.63	0.5
STR28	Rumatianos	22.06	76	6.75	7.18	16.3	36.9	−0.06	0.26	0.18
STR8	Litheos	41.98	77	6.39	6.13	20.6	8.2	−0.31	0.26	0.2
STR14[R]	Gazanos	186.8	54	6.32	11.86	36.9	111.8	−3.05	0.23	0.17
STR1	Patelis	84.57	56	5.91	6.12	12.1	13.7	0.48	0.57	0.51
STR4	Kalamafkianos	36.14	10	5.41	3.57	40.7	10.4	−1.33	0.32	0.3
STR15	Baritis	105.5	44	4.08	3.06	13.2	61.7	−0.04	0.19	0.12
STR25	Agios Vasiliou	35.64	74	2.37	4.62	28	103.4	−2.38	0.26	0.2
STR16	Arvis	26.53	80	1.66	1.14	11.1	11.2	0	0.32	0.23
STR12[R]	Iniotis	105.9	44	1.56	2.21	23.7	57.3	−0.81	0.16	0.12

[R] Gauging stations used in the validation of regionalization technique.
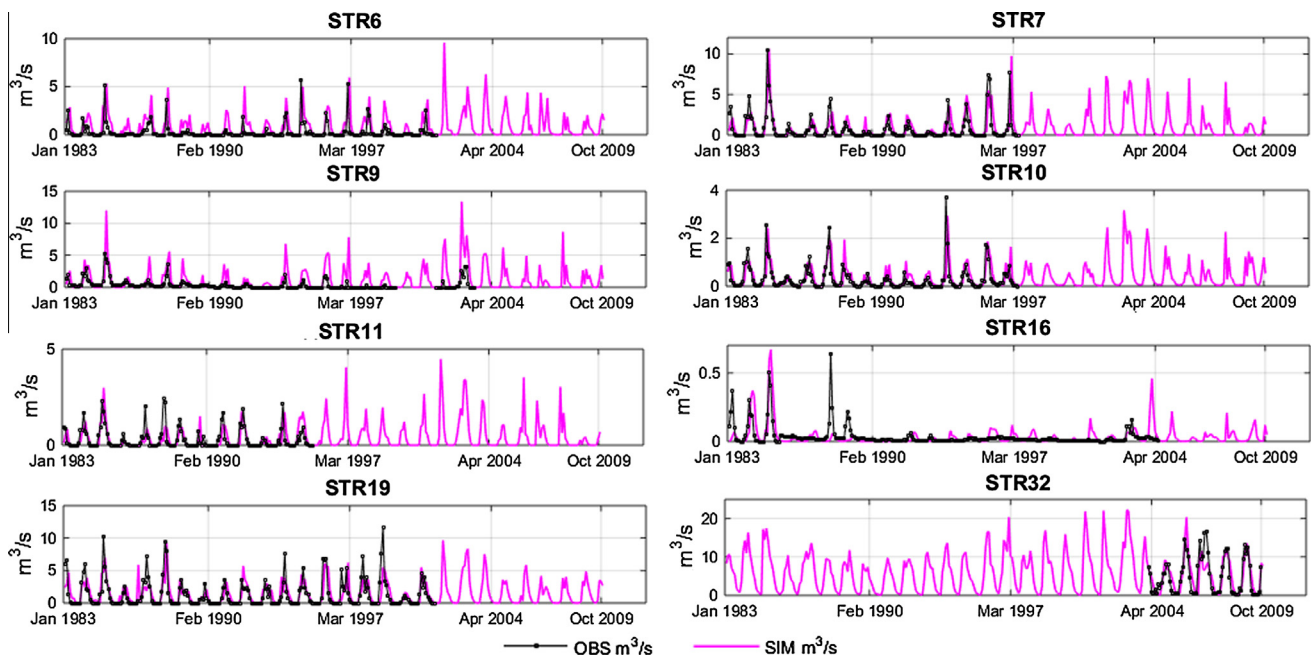

Fig. 5. Some examples, comparison between monthly simulated and observed streamflow values from 1983 to 2009 after the allocation of springs in the SWAT model.
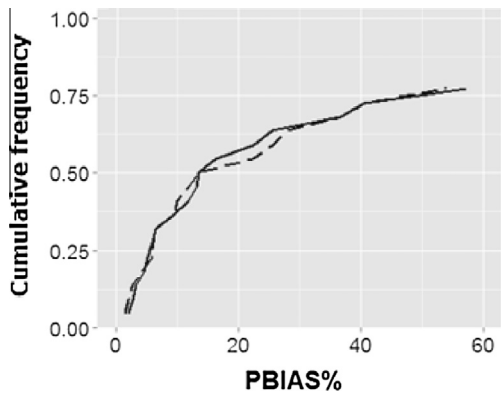
Fig. 6. Cumulative frequency curves of percent bias (PBIAS, %) obtained between monthly and observed streamflow before (only adapting SWAT model) and after the introduction of springs (KSWAT).

basin allowed the automatic assignation of the NOP of "donor subbasins" to the classified ungauged subbasins.

In order to verify the strength of the parameters regionalization in the ungauged subbasins the model performance was evaluated using the percent bias (PBIAS; Gupta et al., 1999) between monthly observed and simulated streamflow at seven gauging stations. This was an intermediate validation that anticipated a final complete validation performed in all gauging stations after the introduction of springs in the model as described in the next paragraphs.

2.4.6. The calibration of springs and delineation of karst recharge area of each spring

The springs were calibrated using the daily recharge of deep aquifer (DA_RCHRG) from the *adapted SWAT model*, except for Spring SP54 (Almiros Heraklion) that was calibrated using DA_RCHRG at monthly time step. The springs were calibrated manually changing parameters of the *karst-flow model* in reasonable ranges: the initial karst flow (m^3/day), the fractions a_1, a_2, and the recession constants k_u and k_l (1/d) for each reservoir as show in Table 2. This process ended when the Normalized Root Mean

Square Error (NRMSE) calculated using the simulated and observed values for each spring was minimized.

42 springs out of 47 were calibrated having hypothesized that some springs drained the same karst area. This assumption was strongly correlated to the neighborhood location of these springs that didn't allow distinguishing the contribution of deep aquifer recharge from the same karst-subbasins; hence SP12 and SP13, SP44 and SP45, SP4 and SP50, SP7, SP18 and SP19 were grouped into SP12-13, SP44-45, SP18-19-7 and SP4-50.

The springs were entered as points sources in the model and the associated calibrated monthly Q_k (m^3/s) were implemented as input data in SWAT. For each spring the karst recharge areas (inside and outside the hydrological boundary) was defined as sum of subbasins areas whose deep aquifer recharge contributes to a specific spring.

The subbasins that contributed to spring flow through their deep aquifer recharge in the *karst-flow model* were not necessarily hydrologically connected. The linkage between these subbasins and the springs represented the movement of water through the cave systems whose spatial extent and organization was different from the surface subbasin hydrologic boundaries.

The performances of the *karst-flow model* were evaluated by visual comparison of measured and simulated hydrographs of springs and using performance indicators including the Normalized Root Mean Square Error (NRMSE), the percent bias (PBIAS; Gupta et al., 1999), the coefficient of determination r^2 multiplied by the slope of the regression line between simulated and observed values (br^2; Krause et al., 2005) to overcome the intrinsic weakness of each indicator (Bennett et al., 2013).

2.4.7. Final calibration and complete validation

After the introduction of calibrated springs in the SWAT model as point sources, an additional manual calibration was necessary to adjust the water discharge including peaks and baseflow since the addition of the spring contribution modified the already calibrated discharge. In particular, the effective hydraulic conductivity in main channel (mm/hr) in Messera, Anapodiaris and in Petras Basins was adjusted (Table 2).
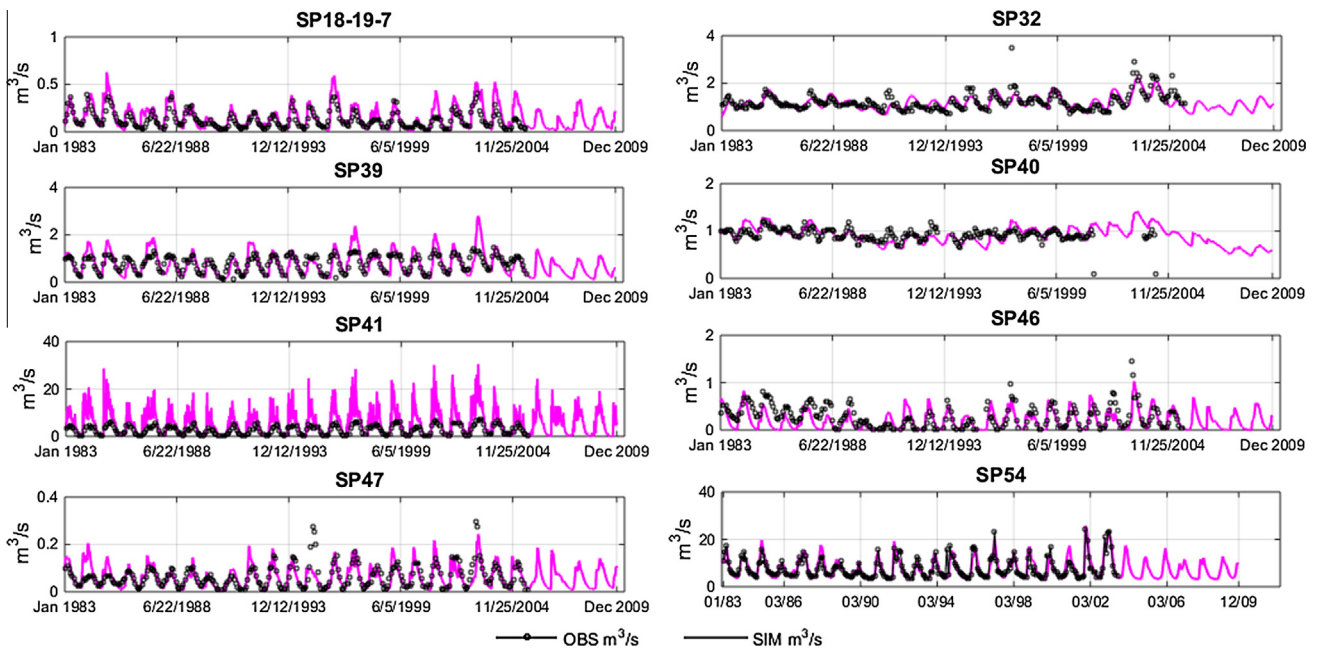

Fig. 7. Some examples, comparison between daily simulated and observed spring's values from 1983 to 2009 (monthly comparison for SP54).

Finally, the complete SWAT model was validated using the whole dataset of streamflow gauging stations in order to evaluate the model performance after the introduction of the springs. Similarly to calibrated streamflow and spring's discharges, the complete SWAT model was validated comparing monthly observed and simulated streamflow in the period 1983–2009 calculating the NRMSE (%), PBIAS (%), the Nash Sutcliffe efficiency (NSE), br^2 and r^2.

3. Results and discussion

3.1. Hydrological simulation

The performance indicators obtained comparing the monthly observed and simulated streamflow for the 22 stream gauging stations after calibration, regionalization and the introduction of the calibrated springs are summarized in Table 3.

It is noteworthy that about 64% of the calibrated gauging streamflow stations reached satisfactory PBIAS% (values in the range ± 25%), while only 40% had NSE greater than 0.5 (see Moriasi et al., 2007 for performance rating as reference). Furthermore, 50% and 36% of calibrated streamflow gauging stations reached respectively r^2 and br^2 larger than 0.5.

Fig. 5 shows some examples of comparison of hydrographs. Even though some of the statistical indicators did not score very high, the hydrographs comparison illustrates that the model was able to reproduce accurately the monthly variations over a long period of simulation even in subbasins influenced by excessive water pumping, such as STR16.

This gauging station was fed by precipitation and discharge of spring SP16. After the year 1990, the spring's discharge was diverted to supply domestic uses reducing drastically the streamflow in particular during the summer and autumn.

It was estimated that the percentage of streamflow gauging stations that reached satisfactory PBIAS (PBIAS < ±25%, Moriasi et al., 2007) increased from 59% to 64% adding spring's discharges in the SWAT model highlighting the significant influence of springs in the water balance of Crete. Fig. 6 shows the PBIAS cumulative curves of performance indicators calculated between monthly

Table 4
Comparison of observed and simulated spring discharges in the period 1983–2009: in the first two columns the code and name of the stations; in the third the karst area that contributes of each spring (km^2) and involves the area inside the hydrological basin and outside; the % data represents the percentage of observed values (once a month) in the period 1983–2009 (324 total months); the observed and simulated volumes are respectively Mm^3/year OBS and SIM; the performance indicators calculated between daily observed and simulated spring discharges are the normalized root mean square error (NRMSE%), the percent bias (PBIAS%), the Nash Sutcliffe Coefficient (NSE), the coefficient of determination (r^2) and the coefficient of determination multiplied by the slope of the regression line between simulated and observed values (br^2).

Station	Name	Estimated karst recharge area (km^2)	% data	Mm^3/year OBS	Mm^3/year SIM	NRMSE %	PBIAS %	NSE	r^2	br^2
SP54[a]	Almiros-Heraklion	323.48	77	235.72	236.59	9.8	0.7	0.77	0.8	0.8
SP41	Stylos	185.01	79	85.81	168.85	66	102.7	−4.8	0.64	0.31
SP9	Almiros-Agios-Nikolaos	155.42	80	83.22	83.73	15.9	3.9	0.22	0.54	0.56
SP43	Platanos/kalamionas-Agia	110.18	10	67.11	67.43	23.8	6.1	0.18	0.55	0.59
SP32	Kourtaliotis	103.37	84	37.99	37.08	9.9	−0.8	0.44	0.43	0.45
SP42	Meskla	114.2	84	30.7	30.94	17.4	11.2	0.31	0.32	0.38
SP40	Kourbos	53.32	68	29.85	28.68	14.6	2.1	−0.61	0.12	0.12
SP38	Vrisses	20.21	77	26.95	26.53	13.4	−3	0.48	0.41	0.51
SP39	Armenoi	78.48	84	24.79	24.09	26.1	1.2	−0.08	0.5	0.5
SP37	Petres	26.2	70	13.77	13.76	15.2	2	0.34	0.26	0.39
SP44_45	Elliniki-Konto Kinigi	40.32	84	13.5	13.52	9.5	5.3	0.44	0.32	0.45
SP34	Spilianos	34.07	84	12.65	11.24	10.7	−6.3	0.36	0.21	0.36
SP36	Mousela Xalikouti	47.95	77	11.95	11.26	9.4	18.9	0.24	0.36	0.41
SP46	Drapania	40.9	75	9.87	6.35	14.9	−21.9	0.16	0.21	0.32
SP48	Therisos	12.6	42	9.68	9.35	16.6	−3	0.32	0.18	0.32
SP28	Geropotamos	25.58	64	7.75	7.81	14.2	−2.5	0.13	0.13	0.22
SP2	Zakros	28.45	80	5.4	5.77	9.5	−1.8	0.62	0.59	0.63
SP3	Chochlakies	34.75	49	5.33	5.47	17.3	2.3	0.34	0.38	0.46
SP27	Panormos Almiro Nero	16.74	69	4.68	4.65	13.1	4	0.07	0.49	0.5
SP18_19_7	Kria Vrisi-Simis-Kefalovrisi Viannou	35.14	84	4.65	4.74	20.6	26.7	0.17	0.55	0.67
SP22	Fodele	22.45	84	3.78	3.99	8.7	−3.2	0.21	0.13	0.22
SP52	Argiroupoli	24.23	44	3.67	3.54	18.7	18.7	0.09	0.51	0.6
SP49	Kefalovris/Kalamoukas-Ierapetra	17.91	84	3.54	3.59	10	−4.8	0.41	0.33	0.46
SP12_13	Almiros Mallia-Grammatikaki	22.89	80	3.51	3.43	12.7	10.4	0.49	0.48	0.56
SP6	Archon Stavrochoriou – Sitia	28.91	83	3.26	3.23	12.5	−1.7	0.38	0.49	0.51
SP20	Zaros – Votomos	26.38	10	3.15	3.03	32.4	−0.1	−0.06	0.04	0.04
SP30	Spili	14.21	21	3.07	3.1	30.4	−2	−0.85	0.1	0.11
SP8	Kalo Chorio	14.61	76	3.05	3.1	14.3	1.2	0.29	0.26	0.3
SP11	Zou	29.54	48	2.14	2.14	13.2	−14.7	0.51	0.35	0.52
SP47	Sfinari	32.57	84	1.96	1.99	12.8	−0.2	0.42	0.43	0.49
SP31	Agia Fotia-Spili	14.21	35	1.94	1.97	21.4	−9.7	0.29	0.26	0.36
SP25	Emparos	16.14	36	1.53	1.52	13	11.5	−0.11	0.01	0.02
SP26	Seises	2.5	80	1.53	1.23	16.7	−20.9	0.05	0.3	0.4
SP4_50	Agios Georgios Sitia-Sikia Sitia	18.27	42	1.52	1.49	23.8	103.4	−1.06	0.26	0.35
SP21	Gergeri	41.8	17	1.49	1.86	14.8	−8.3	0.57	0.57	0.63
SP35	Ligres	8.35	17	1.46	1.41	14.7	14	0.41	0.46	0.47
SP5	Lithines-Sitia	18.73	81	1.38	1.31	11.9	−3.6	0.54	0.42	0.56
SP14	Avli Migilisi	18.85	4	1.15	1.02	50.7	43.8	−1.04	0.41	0.62
SP51	Loutraki	33.22	58	1.09	1.19	19.1	27.2	−0.1	0.42	0.49
SP10	Petikou	3.22	80	1.01	1.02	8.1	11.5	0.62	0.56	0.63
SP16	Mega Vrisi	28.97	34	0.65	0.64	20.3	32.7	0.04	0.1	0.16
SP53	Agios Georgios-Viannou	3.69	33	0.11	0.2	19.1	7	0.22	0.37	0.39

[a] For SP54 the performance indicators were calculated using monthly values.

and observed streamflow before and after the introduction of springs as point sources in the SWAT model.

In particular, streamflow discharge of gauging stations STR32 (Koiliaris), STR16 (Avli), and STR10 (Koutsoulidis) were strongly influenced by the discharge of springs SP41 (Stylos), SP14-SP25 (Migilisi and Emparos) and SP20 (Zaros), respectively. For STR32 the PBIAS decreased to 3% and the NSE increased to 0.68, for STR16 the PBIAS% reached 11%, and finally for STR10 the PBIAS% and NSE were also satisfactory reaching 17% and 0.83 respectively (Table 3).

These results demonstrated that the *karst-flow model* correctly simulated the discharge of springs increasing the SWAT model performance. Fig. 7 shows some examples of comparison between daily observed and simulated spring flows (only for SP54 monthly comparison), and Table 4 summarizes the comparison between monthly and observed long-term annual discharge on the period 1983–2009 and the performance indicators for all springs. It is noteworthy that for more than 70% of the calibrated springs the PBIAS% is within the range of ±25%, indicating that the performance of the *karst-flow model* was satisfactory (Moriasi et al., 2007). NSE was positive for 80% of calibrated springs, while r^2 and br^2 had a wide range of values with around 50% of the values larger than 0.4.

However, the *karst-flow model* markedly overestimated the discharge for springs SP4-50 (Agios Georgios Sitia-Sikia Sitia), SP14 (Avli Migilisi), SP16 (Mega Vrisi), SP41 (Stylos) and SP51 (Loutraki) maybe due to the quality of the observed data.

Concerning SP41, the most studied spring in Crete (Nikolaidis et al., 2013; Moraetis et al., 2010; Kourgialas et al., 2010), was intentionally calibrated to overestimate the flow in order to take into account the contribution of ungauged springs. Nikolaidis et al. (2013) reported that Stylos spring has two permanent springs at elevation +17 m AMSL (with 85 Mm^3/year of volume), but there was also an ungauged intermittent spring (Anavreti at elevation +24 m AMSL). Both contributed to Koiliaris discharge. The authors argued that these springs have a total average discharge around 154 Mm^3/y (2007–2010), and this volume was in agreement with the total overestimated volume of Stylos in this work (150 Mm^3/y, for the same period 2007–2010, 170 Mm^3/y considering 1983–2009). Finally, it is noteworthy that the spring SP46 (Fig. 7) had two different hydrological behaviors: observed data were higher prior to year 1988, then the values decreased sharply highlighting

changes in the regime of discharge. This may be explained by a change in the method of measurement or more probably by an excessive pumping of water as occurred for the STR16 spring.

3.2. The estimated recharge areas of karst springs

Fig. 8 shows some schematic examples of recharge areas of springs obtained considering the subbasins that contribute with their deep aquifer recharge to the calibration of springs. Table 4 summarized also the karst recharge areas (km^2) for each spring or group of springs. The karst recharge areas of springs cover karst-subbasins and karst areas for a total of 1928 km^2, about the 70% of total karst areas in Crete. The main karst recharge area drains more than 300 km^2 into Almiros Heraklion Spring (SP54), followed by the karst recharge area of Almiros-Agios-Nikolaos Spring (SP9) that cover about 155 km^2, and 130 km^2 of karst recharge area of springs in Koiliaris Basin.

To the best of our knowledge this work was the first estimation of karst recharge areas of all gauged springs in the Island of Crete, providing valuable information for water resources management. The only exception was the karst area drained by Almiros Spring and the knowledge of extended areas (outside the hydrological boundary of basin) of springs in Koiliaris Basin.

Bonacci and Fistanic (2006) pointed out the difficulties to define the karst area drained by Almiros Spring due to complex geology and hydrogeology. There were different assumptions of its boundaries and size which varies from 300 km^2 (Arfib et al., 2000) to 500 km^2 (Lambrakis et al., 2000). However, Bonacci (1995) and Bonacci and Ljubenkov (2005) estimated the karst recharge area of Almiros of about 300 km^2, similar to our finding.

The area outside the Koiliaris Basin that contributed to the karst recharge area of Stylos Spring and other ungauged springs in Koiliaris Basin was estimated around 80 km^2 (7 subbasins that contribute with 70% of their total area). As a consequence, more than 60% of karst recharge area of Koiliaris springs was outside the boundary of the hydrological basin. This result was confirmed by Nikolaidis et al. (2013) that estimated an extended karst area of springs in Koiliaris Basin of 79 km^2 based on hydrologic modeling and geologic cross-sections.

Albeit this approach may be criticized by the fact that karst recharge areas should be only delineated based on hydrogeological considerations derived, i.e. by tracer tests, it has to be taken into
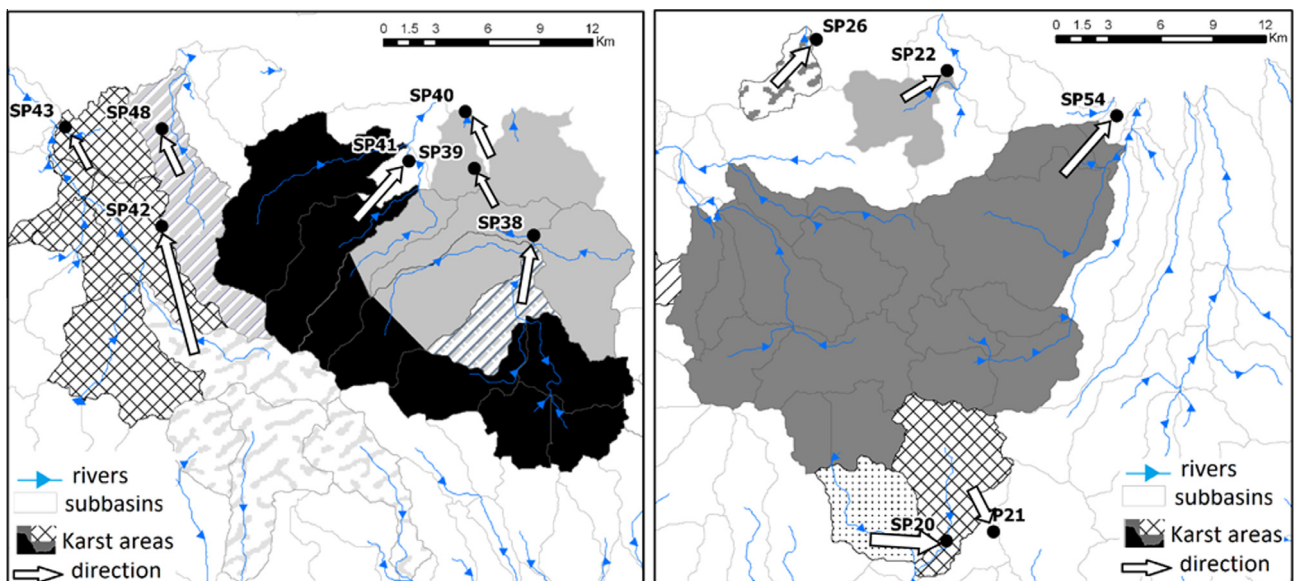

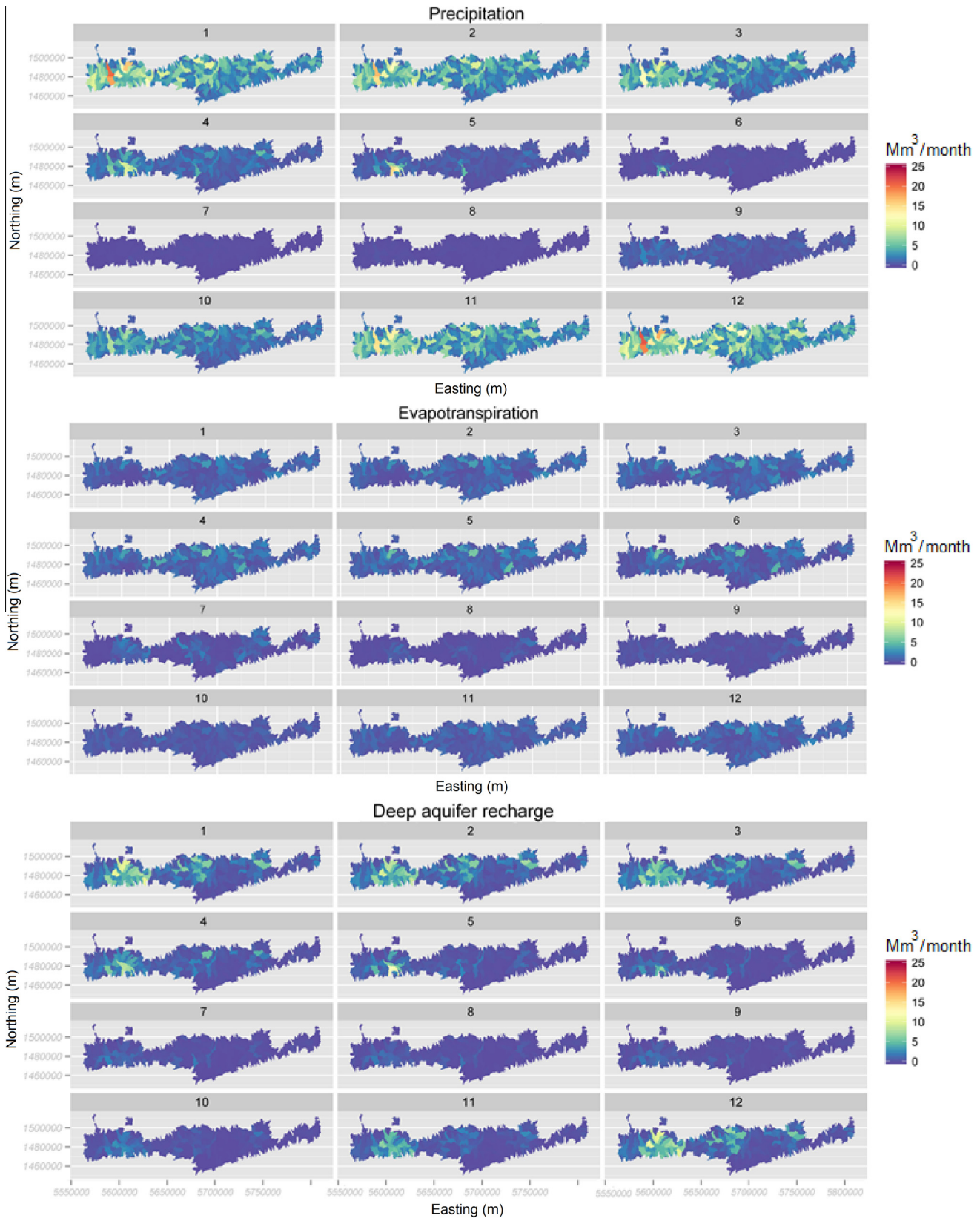**Fig. 8.** Examples of estimated karst recharge area of selected springs.

Fig. 9. Maps of monthly variations of precipitation, evapotranspiration and the deep aquifer recharge (Mm^3/month).

account that there are limits in the use of tracer studies in karst areas such as in Koiliaris basin. In a geological karst area which discharges a large volume of water there is a risk of high degree of

dilution of tracers (Knithakis, 1995) which in turn limits the usefulness of the methods in delineating the extend area. In addition, breakthrough curves are highly dependent on the flow conditions,
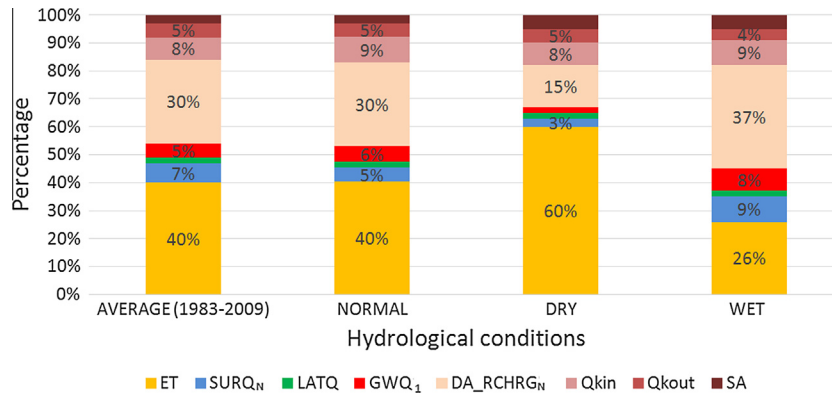
Fig. 10. Annual water balance in different hydrological conditions (in percentage), average of 27 years (total volume of precipitation 6370 Mm^3/y), normal year (total volume of precipitation 6400 Mm^3/y), dry year (total volume of precipitation 3700 Mm^3/y) and wet year (total volume of precipitation 9600 Mm^3/y). ET, evapotranspiration; $SURQ_N$, surface runoff excluding losses from tributaries and wetlands; LATQ, lateral flow; GWQ_1, baseflow; DA_RCHRG_N, amount of water recharge in the deep aquifer without the contribution for springs that discharge inside (Qkin) and outside (Qkout) Crete Watershed; SA, shallow aquifer storage.

often necessitating the repetition of the tracing experiment under low flow and high flow conditions as observed by Goldscheider (2005) and Ravbar et al. (2011).

3.3. Spatial and temporal variation of hydrological components in Crete

The mean annual precipitation ranges from 550 mm (driest year) to 1400 mm (wettest year) during the period 1983–2009, with a decreasing gradient from west to east. The precipitation was higher at high elevation, reaching more than 2500 mm in the wet years (1996, 1997, 2001 and 2003) and around 1000 mm in the central north areas, while in the plain areas and along the south cost the average annual rainfall was below 1000 mm.

The mean calculated actual evapotranspiration of Crete varied from 340 mm/y (driest year) to 390 mm/y (wettest year) reaching the maximum values long the north coast and, in particular in Karteros, Aposelemis, Tzermiadon, Myrtos and Anapodiaris basins (east-central part of Crete).

Large values of surface runoff were simulated in the western part of Crete and in particular in Tavronitis Basin with maximum value in wet years, such as in 1997 and 2003 (more than 1100 mm). Minor contributors to the water balance include lateral flow and baseflow. The baseflow reached high values in Kourtaliotis, Akoumianos and Platis basins (south-central Crete). The annual and spatial variations of deep aquifer recharge were strongly correlated to the precipitation, as a consequence in zones with high precipitation the deep aquifer recharge reached the largest values since the main mountainous systems were associated with the most important karst systems, allowing water to penetrate directly to the deep aquifer as showed in Fig. 9. In particular, Fig. 9 illustrates how precipitation, evapotranspiration and recharge of the deep aquifer change during the year. Precipitation and deep aquifer recharge changed during the year decreasing from January (~1120 and 463 Mm^3/month respectively) to August (~18 and 62 Mm^3/ month respectively) and increasing from September (~163 and 63 Mm^3/month respectively) to December (~1250 and 416 Mm^3/ month respectively). During the wettest months, the west part of Crete reached the highest values of precipitation and also the highest value of deep aquifer recharge. The evapotranspiration increased from January (~240 Mm^3/month) to April (~320 Mm^3/ month), in particular in subbasins long the cost, and then decreased until August (~54 Mm^3/month) and increased from September (~71 Mm^3/month) to December (~240 Mm^3/month). These long-term spatially and monthly variations could be very

useful for planning and implementing conservations measures and programs and evaluating their performance.

3.4. The estimated water balance of Crete

Chartzoulakis et al. (2001) and many other studies (RCG, 2002; Vardavas et al., 2004; MEDIWAT, 2013; Koutroulis et al., 2013; Baltas and Tzoraki, 2013) pointed out the importance of the evapotranspiration on the water balance of the whole Crete giving infiltration a secondary role. Conversely to these findings, the Crete SWAT model has allowed the estimation of the water balance of Crete resulting in significantly different estimates. Fig. 10 summarizes the percentage of flow contribution of the water balance main components with respect to the long-term average volumes and different hydrological conditions during the period 1983–2009. In addition, Fig. 11 represents the previous results following the KSWAT model approach providing a more readable and systematic information of the fluxes.

The evapotranspiration volume ranged from around 2250 Mm^3/y in the driest year to 2500 Mm^3/y in the wettest year exhibiting a small variation in terms of absolute values but with a significant variation with respect to the total volume of precipitation (Fig. 10). In the wettest year the main component of hydrological processes was the deep aquifer recharge, while in the driest year the evapotranspiration had the main role. From dry to wet year the surface runoff increased from 95 Mm^3/y to more than 800 Mm^3/y and the total net water available in the deep aquifer increased from 550 Mm^3/y to around 3500 Mm^3/y in dry and wet year, respectively.

As a consequence, during the wet conditions there was high infiltration, but also the surface runoff was larger than that during driest and normal hydrological condition. On the other hand, in dry years there was also significant percolation to the deep aquifer (1000 Mm^3/y). This result was also highlighted by Hartmann et al. (2014, 2015) pointing out that karst regions might be more resilient to climate change in terms of both flooding and droughts. Furthermore, the authors demonstrated the existence a nonlinear relationship between precipitation and recharge rate indicating that the recharge of deep aquifer is more sensitive to a decrease than to an increase of precipitation (Hartmann et al., 2014). This was confirmed also in this study where the total deep aquifer recharge was estimated 28% of precipitation in driest year, while was 50% in wettest year departing of 16% and 6% from normal conditions, respectively.

Concerning the percentage of water balance components (Fig. 11), it was estimated that from the total precipitation of
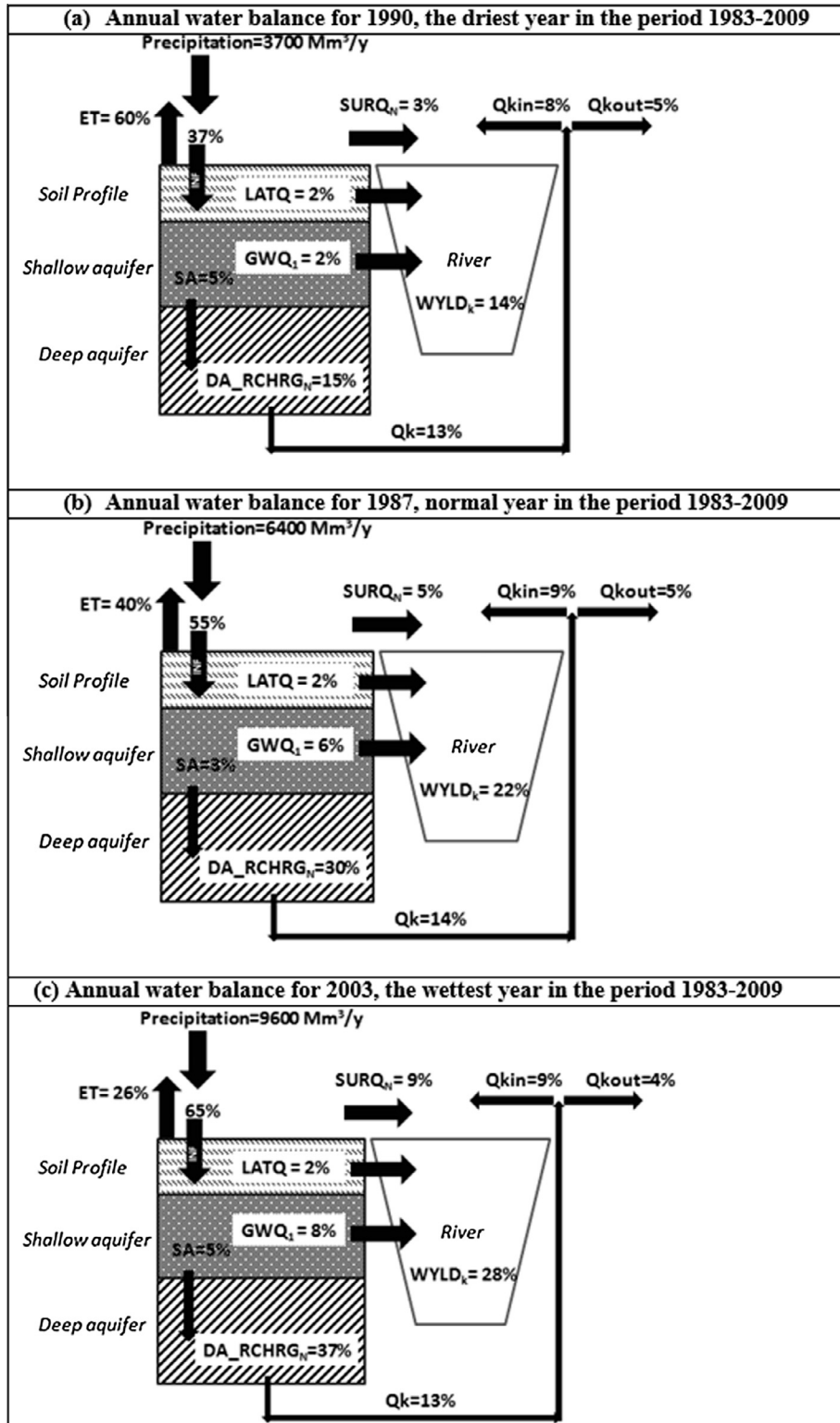
Fig. 11. Annual water balance schematization in different hydrological conditions, dry (a), normal (b) and wet (c) year. ET, evapotranspiration; INF, infiltration in the soil; SURQ_N, surface runoff excluding the losses from tributaries and wetlands; LATQ, lateral flow; GWQ_1, baseflow; DA_RCHRG_N, amount of water recharge in the deep aquifer without the contribution for springs that discharge inside (Qkin) and outside (Qkout) Crete; WYLD_k, freshwater contribution; SA, shallow aquifer storage.

6400 Mm^3/y about 40% was lost through evapotranspiration, 55% infiltrates and only 5% was surface runoff. The surface runoff including lateral flow (LATQ), baseflow (GWQ$_1$) and spring's discharge (Qkin) contribution to streamflow represents 22% of total precipitation. The total amount of deep aquifer recharge was around 44% of which 14% contributed as springs discharge to streamflow (Q_{in} = 9%) or sea (Q_{out} = 5%) (Fig. 11b). These percentages were valid for all years in normal hydrological conditions (for instance year 1987), but they changed in extreme hydrological conditions.

Considering the driest year (year 1990, Fig. 11a), it was estimated that from the total precipitations of 3700 Mm^3/y about 60% was lost through evapotranspiration, 37% infiltrated and only 3% was surface runoff.

The amount of deep aquifer recharge decreased with respect to the normal hydrological condition to 28% of which 13% contributed as springs discharge to streamflow ($Q_{in} = 9\%$) or sea ($Q_{out} = 4\%$). The total contribution to freshwater decreased to 14% with respect to the normal condition.

In the wettest year (year 2003, Fig. 11c), considering a total volume of precipitation around 9600 Mm^3/y, evapotranspiration was estimated around 26%, 65% was infiltration and 9% was surface runoff. The deep aquifer recharge reached the highest percentage of 50% and the water yield increased to 28%. Our work has shown that the evapotranspiration ranged between 2250 Mm^3/y in a driest year and of 2500 Mm^3/y in wettest year, corresponding to 60% and 26% of total precipitation, respectively. These results suggested the importance of karst water supply during dry periods.

3.5. Strengths and challenges of the karst modeling approach

The modeling approach proposed in this study allowed achieving satisfactory simulations of streamflow and springs discharges at monthly and daily time step respectively across the whole Crete Island. These temporal resolutions are inherently linked to the available input data (Table 1), the nature of the simulated hydrologic processes and the modeling objectives (Baffaut et al., 2015). Conversely to previously studies that focus mainly on annual or long-term mean annual prediction (i.e. Malard et al., 2015), here the monthly simulations of streamflow have allowed capturing the seasonal variations and gathering precious information for a better water resources management. Similarly, the daily simulated springs discharges provided information of each karst recharge area and the spring hydrograph, if further investigated, can also express some geometrical and hydraulic characteristics of aquifers (Fiorillo, 2014).

Furthermore, the spatial and temporal (annual and monthly) distribution of simulated water resources (i.e. precipitation, deep aquifer recharge, evapotranspiration and runoff) and the mean annual water balances in different hydrological conditions are important benefits of the present work.

Despite these strengths, the modeling approach suffers from some limits. For instance, the monthly time step of streamflow has limited the application of step-wise calibration not allowing a reliable estimation of each component of the streamflow. Furthermore, in data scarce areas, where only annual time step is available and spatial data has coarse resolutions, the reproducibility of the KSWAT model needs some adaptations that should be evaluated case by case. Likewise, the knowledge of springs discharges and their position is vital and in extremis they could be approximated using literature information. In this context, soft data has an important role and should be seen as injections of some insightful common sense into the automatic or semiautomatic calibration procedure (Seibert and McDonnell, 2002). For instance, Malard et al. (2015) used 42 alpine and peri-alpine specific springs discharges from literature as references sites in Switzerland for karst recharge assessments, and Hartmann et al. (2015) used 40 independent observations of mean annual recharge both from field and modeling studies over Europe and Mediterranean.

Finally, albeit the identification of karst recharge areas of each spring is a valuable aspect of the KSWAT model, the associated uncertainty was not object of this study and this topic deserves further investigations that may involve climatic and topographic descriptors as pointed out in Hartmann et al. (2015).

4. Conclusion

In this study the SWAT model was adapted and integrated with a karst-flow model to simulate the karst water resources in the Island of Crete. The KSWAT model allowed calibrating the daily spring discharges in 47 gauging stations, estimating their karst recharge areas and their introduction in the SWAT model increased the performance of streamflow prediction in karst-subbasins. These springs contributed significantly to total discharge with 300 Mm^3/y in dry hydrological condition, ensuring ecological services (Malard et al., 2015), and 850 Mm^3/y in wet periods. In addition, the seasonal variation of volume of springs suggests that these valuable sources should be conserved and preserved in particular from April to September when available volumes are the lowest and agriculture and tourism demand increases.

The analysis of the water balance also showed that water resources are not homogeneously distributed in Crete and change significantly in different hydrological conditions. In particular, the western part of Crete has a surplus of water resources with respect to the eastern part where there is low water availability and high demand. Messara Valley (Geropotamos Basin) is an example of intensively managed basin in south-eastern Crete where an overexploitation of groundwater is occurring in a large number of wells since 1984 that continue to decrease groundwater levels at alarming proportions (Kritsotakis and Tsanis, 2009).

In this context, the present study provides a methodology and a tool for the integrated water management of Crete and other similar areas, by providing detailed spatially distributed hydrologic balances and accurate estimation of water availability using both hard and soft data.

Acknowledgements

References

Abbaspour, K.C., 2008. SWAT-CUP2: SWAT Calibration and Uncertainty Programs – A User Manual. Department of Systems Analysis, Integrated Assessment and Modelling (SIAM), Eawag, Swiss Federal Institute of Aquatic Science and Technology, Duebendorf, Switzerland.

Abbaspour, K.C., Rouholahnejad, E., Vaghefa, S., Srinivasan, R., Yang, H., Kløve, B., 2015. A continental-scale hydrology and water quality model for Europe: Calibration and uncertainty of a high-resolution large-scale SWAT model. J. Hydrol. 524 (1), 733–752.

Agriculture Statistics of Greece, 2005. ΠΕΙΡΑΙΑΤΜ-2009-PIREAS.

Arfib, B., de Marsily, G., Ganoulis, J., 2000. Pollution by seawater intrusion into a karst system: new research in the case of the Almyros source (Heraklion, Crete, Greece). Acta Carsologica 29 (1), 15–31.

Arnold, J.G., Youssef, M.A., Yen, H., White, M.J., Sheshukov, A.Y., Sadeghi, A.M., Moriasi, D.N., Steiner, J.L., Amatya, D.M., Skaggs, R.W., Haney, E.B., Jeong, J., Arabi, M., Gowda, P.H., 2015. Hydrological processes and model representation: impact of soft data on calibration. Trans. ASABE 58 (6), 1637–1660. http://dx.doi.org/10.13031/trans.58.10726.

Arnold, J.G., Srinivasan, R., Muttiah, R.S., Williams, J.R., 1998. Large area hydrologic modeling and assessment: Part I. Model development. J. Am. Water Resour. Assoc. 34 (1), 73–89.

Baffaut, C., Benson, V.W., 2009. Modeling flow and pollutant transport in a karst watershed with SWAT. Trans. ASABE 52, 469–479.

Baffaut, C., Dabney, S.M., Smolen, M.D., Youssef, M.A., Bonta, J.V., Chu, M.L., Guzman, J.A., Shedekar, V., Jha, M.K., Arnold, J.G., 2015. Hydrologic and water quality modeling: spatial and temporal considerations. Trans. ASABE 58 (6), 1661–1680. http://dx.doi.org/10.13031/trans.58.10714.

Bakalowicz, 2015. Karst and karst groundwater resources in the Mediterranean. Environ. Earth Sci. 74, 5–14.

Baltas, E., Tzoraki, O., 2013. Water Resources Management on the Island of Crete: Lessons Learnt. In: United Nations International Year of Water Cooperation (Eds.), Free Flow – Reaching Water Security Through Cooperation, Tudor Rose. p. 285–9.

Bartholome, E., Belward, A.S., 2005. GLC2000: A new approach to global land cover mapping from Earth observation data. Int. J. Remote Sens. 26 (9), 1959–1977.

Bashfield, A., Keim, A., 2011. Continent-wide DEM creation for the European Union. In: 34th International Symposium on Remote Sensing of the Environment, Sydney, Australia, 10–15 April 2011 <http://www.isprs.org/proceedings/2011/ISRSE-34/211104015Final00143.pdf> (accessed 21st January 2015); data available at <http://www.eea.europa.eu/data-and-maps/data/eu-dem#tab-metadata> (accessed 21st January 2015).

Bennett, N.D., Croke, B.F.W., Guariso, G., Guillaume, J.H.A., Hamilon, S.H., Jakeman, A.J., Marsili_libeli, S., Newham, L.T.H., Norton, J.P., Perrin, C., Pierce, S.A., Robson, B., Voinov, A.A., Fath, B.D., 2013. Characterising performance of environmental models. Environ. Model. Softw. 40, 1–20.

Bonacci, O., 1995. Brackish karst spring Pantan. Acta Carsologica 24, 97–107.

Bonacci, O., Fistanic I., 2006. Contribution to hydrological analysis of the coastal karst spring Almyros (Creete, Greece). In: Conference on Water Observation and information system for decision support, Balwois (Ohrid, Republic of Macedonia). Radic (Eds.), UNDP-Agency of Skopje. p. 191–2.

Bonacci, O., Ljubenkov, I., 2005. Nova saznanja o hidrologiji rijeke Krke. Hrvatske Vode 13 (52), 265–281.

Bouraoui, F., Aloe, A., 2007. European Agrochemicals Geospatial Loss Estimator: Model development and Applications, EUR – Scientific and Technical Research Series, ISSN 1018-5593. Office for Official Publications of the European Communities, Luxembourg.

Britz, W., 2004. CAPRI Modeling System Documentation. Final Report of the FP5 Shared Cost Project CAP-STRAT "Common Agricultural Policy Strategy for Regions, Agriculture and Trade." QLTR-2000-00394. Univ. Bonn, Bonn, Germany.

Britz, W., Witzke, P., 2008. CAPRI Model Documentation 2008: Version 2. In: Britz, W., Witzke, P. (Eds.). Bonn: University of Bonn, Institute for Food and Resource Economics.

Buchanan, T.J., Somers, W.P., 1976. Discharge measurements at gaging stations. Techniques of Water-Resources Investigations of the United States Geological Survey. Washington, D.C.: USGS. Book 3, Chapter A8.

Chartzoulakis, K.S., Paranychianakis, N.V., Angelakis, A.N., 2001. Water resources management in the island of Crete, Greece, with emphasis on the agricultural use. Water Pol. 3 (3), 193–205.

Daly, D., Dassargues, A., Drew, D., Dunne, S., Goldscheider, N., Neale, S., Popescu, C., Zwhalen, F., 2002. Main concepts of the "European Approach" for (karst) groundwater vulnerability assessment and mapping. Hydrogeol. J. 10 (2), 340–345.

Dettling, M., Maechler, M., 2012. Supclust: Supervised clustering of predictor variables such as genes. R package version 1.0-7.

EC, 2003. Vulnerability and risk mapping for the protection of carbonate (Karst) aquifers 2003. In: Zwahlen, F. (Ed.), COST-620 Action Final Report. European Commission, DG-Research, p. 320.

EC, 2004. The main coastal karstic aquifers of southern Europe 2004. In: Calaforra, J. M., (Ed.), COST-621 Action, Groundwater Management of Coastal Karstic Aquifers, European Commission, DG-Research, 126.

EU-DEM, Metadata <http://www.eea.europa.eu/data-and-maps/data/eu-dem#tab-metadata>.

European Soil Portal, 2014 <http://eusoils.jrc.ec.europa.eu/ESDB Archive/ESDB/> (accessed April 2014).

FAO, 2008. Harmonized World Soil Database (version 1.0). FAO, Rome. Italy and IIASA, Laxenburg, Austria.

Fiorillo, F., 2014. The recession of spring hydrographs, focused on karst aquifers. Water Resour. Manage. 28, 1781–1805.

Goldscheider, N., 2005. Fold structure and underground drainage pattern in the alpine karst system Hochifen-Gottesacker. Eclogae Geol. Helv. 98 (1), 1–17. http://dx.doi.org/10.1007/s00015-005-1143-z.

Gupta, H.V., Sorooshian, S., Yapo, P.O., 1999. Status of automatic calibration for hydrologic models: comparison with multilevel expert calibration. J. Hydrol. Eng. 4 (2), 135–143.

Hartmann, A., Gleeson, T., Rosolem, R., Pianosi, F., Wada, Y., Wagener, T., 2015. A large-scale simulation model to assess karstic groundwater recharge over Europe and the Mediterranean. Geosci. Model Dev. 8, 1729–1746. http://dx.doi.org/10.5194/gmd-8-1729-2015.

Hartmann, A., Mudarra, M., Andreo, B., Marín, A., Wagener, T., Lange, J., 2014. Modeling spatiotemporal impacts of hydroclimatic extremes on groundwater recharge at a Mediterranean karst aquifer. Water Resour. Res. 50 (8), 6507–6521. http://dx.doi.org/10.1002/2014WR015685.

Klein, G.K., van Drecht, G., 2006. HYDE 3: Current and historical population and land cover. In: Integrated Modeling of Global Environmental Change. An Overview of IMAGE 2.4.93-111. Netherlands Environmental Assessment Agency (MNP), Bilthoven, The Netherlands.

Klemeš, V., 1986. Dilettantism in hydrology: transition or destiny. Water Resour. Res. 22 (9), 177S–188S.

Knithakis, M., 1995. Hydrogeological Investigation of Rethymnon Region (Prefecture of Rethymnon). Institute of Geological and Mineralogical Investigations (IGME), Rethymnon.

Kourgialas, N.N., Karatzas, G.P., Nikolaidis, N.P., 2010. An integrated framework for the hydrologic simulation of a complex geomorphological river basin. J. Hydrol. 381, 308–321.

Koutroulis, A.G., Tsanis, I.K., Jacob, D., 2013. Impact of climate change on water resources status: a case study for Crete Island, Greece. J. Hydrol. 479, 146–158. http://dx.doi.org/10.1016/j.jhydrol.2012.11.055.

Krause, P., Boyle, D.P., Base, F., 2005. Comparison of different efficiency criteria for hydrological model assessment. Adv. Geosci. 5, 89–97.

Kritsotakis, M., Tsanis, I.K., 2009. An integrated approach for sustainable water resources management of Messara Basin, Crete, Greece. EWRA 27 (28), 15–30.

Lambrakis, N., Andreou, A.S., Polydoropoulos, P., Georgopoulos, E., 2000. Nonlinear analysis and forecasting of a brackish karstic spring. Water Resour. Res. 36 (4), 875–884.

Malagò, A., Pagliero, L., Bouraoui, F., Franchini, M., 2015. Comparing calibrated parameter sets for the Scandinavian Peninsula and for the Iberian Peninsula. Hydrol. Sci. J. 60 (5), 949–967. http://dx.doi.org/10.1080/02626667.2014.97833.

Malard, A., Sinreich, M., Jeannin, P., 2015. A novel approach for estimating karst groundwater recharge in mountainous regions and its application. Hydrol. Process. http://dx.doi.org/10.1002/hyp.10765.

MEDIWAT, 2013. State of the art of Water Resources in Mediterranean Islands. Available at: <http://www.mediwat.eu/sites/default/files/D.3.1.1.pdf>.

Mevic, B., Wehrens, R., 2007. The pls package: principal component analysis and partial least squares regression in R. J. Stat. Softw. 18 (2), 1–23.

Monfreda, C., Ramankutty, N., Foley, J., 2008. Farming the planet: 2. Geographic distribution of crop areas, yields, physiological types, and net primary production in the year 2000. Global Biogeochem. Cycles 22, GB1022.

Moraetis, D., Efstathiou, D., Stamati, F., Tzoraki, O., Nikolaidis, N.P., Schnoor, J.L., Vozinakis, K., 2010. High frequency monitoring for the identification of hydrological and biochemical processes in a Mediterranean river basin. J. Hydrol. 389, 127–136.

Moriasi, D.N., Arnold, J.G., Van Liew, M.W., Bingner, R.L., Harmel, R.D., Veith, T.L., 2007. Model evaluation guidelines for systematic quantification of accuracy in watershed simulations. Trans. ASABE 50, 885–900.

Nash, J.E., Sutcliffe, J.V., 1970. River flow forecasting through conceptual models. Part I: a discussion of principles. J. Hydrol. 10, 282–290.

Neitsch, S.L., Arnold, J.G., Kiniry, J.R., Srinivasan, R., Williams, J.R., 2010. Soil and Water Assessment Tool Input/Output File Documentation Version 2009, Grassland. Soil and Water Research Laboratory, Agricultural Research Service and Blackland Research Center, Texas Agricultural Experiment Station, College Station, Texas.

Nikolaidis, N.P., Bouraoui, F., Bidoglio, G., 2013. Hydrologic and geochemical modeling of a karstic Mediterranean watershed. J. Hydrol. 477, 129–138.

Ntegeka, V., Decloedt, L.C., Willems, P., Monbaliu, J., 2012. Quantifying the impact of climate change from inland, coastal and surface conditions. In: Klijn, F., Schweckendiek, T. (Eds.), Comprehensive Flood Risk Management – Research for Policy and Practise, CRC Press, Taylor & Francis Group, Leiden, The Netherlands; In: Proceedings of the 2nd European Conference on Flood Risk Management FLOODRisk 2012, Rotterdam, The Netherlands, 19–23 November 2012.

Oudin, L., Kay, A., Andréassian, V., Perrin, C., 2010. Are seemingly physically similar catchments truly hydrologically similar? Water Resour. Res. 46, W11558. http://dx.doi.org/10.1029/2009WR008887.

Pagliero, L., Bouraoui, F., Willems, P., Diels, J., 2015. Large-scale hydrological simulations using the soil water assessment tool, protocol development, and application in the Danube Basin. J. Environ. Qual. 43, 145–154.

Parajka, J., Merz, R., Bloschl, G., 2005. A comparison of regionalisation methods for catchment model parameters. Hydrol. Earth Syst. Sci. 9, 157–171.

PHU 2007. POTENTIAL HEAT UNIT (PHU) PROGRAM download <http://swat.tamu.edu/software/potential-heat-unit-program/> (accessed 21st January 2007).

Rantz, S.E., et al., 1982. Measurement and Computation of Streamflow: Volume 1. Measurement of Stage and Discharge. U.S. Geological Survey Water-Supply Paper 2175.

Ravbar, N., Engelhardt, I., Goldscheider, N., 2011. Anomalous behaviour of specific electrical conductivity at a karst spring induced by variable catchment boundaries: the case of the Podstenjšek spring, Slovenia. Hydrol. Process. 25 (13), 2130–2140. http://dx.doi.org/10.1002/hyp.7966.

RGC, 2002. Integrated Water Resources Management on Crete. Study Made Under the Department of Water Resources Management (in Greek).

Sawicz, K., Wagener, T., Sivapalan, M., Troch, P.A., Carillo, G., 2011. Catchment classification: empirical analysis of hydrologic similarity based on catchment function in the eastern USA. Hydrol. Earth Syst. Sci. 15, 2895–2911.

Seibert, J., McDonnell, J.J., 2002. On the dialog between experimentalist and modeler in catchment hydrology: use of soft data for multicriteria model calibration. Water Resour. Res. 38 (11), 23.1–23.14.

Shamir, E., Iman, B., Morin, E., Gupta, H.V., Sorooshian, S., 2005. The role of hydrograph indices in parameter estimation of rainfall–runoff models. Hydrol. Process. 19, 2187–2207.

Smart, C.C., Worthington, S.R.H., 2004. Springs. In: Gunn, J. (Ed.), Encyclopedia of Caves and Karst Science. Fitzroy Dearbon, London, pp. 699–703.

Steiakakis, E., Monopolis, D., Vavadakis, D., Lambrakis, N., 2011. Effective infiltration assessment in Kourtaliotis karstic basin (S. Crete). Adv. Res. Aquatic Environ., 485–492

Taylor, R., 1990. Interpretation of the correlation coefficient: a basic review. J. Diagn. Med. Sonog. (January/February), 35–39

Tzoraki, O., Nikolaidis, N.P., 2007. A generalized framework for modeling the hydrologic and biogeochemical response of a Mediterranean temporary river basin. J. Hydrol. 346, 112–121.

van Griensven, A., Meixner, T., Grunwald, S., Bishop, T., Diluzio, M., Srinivasan, R., 2006. A global sensitivity analysis tool for the parameters of multi-variable catchment model. J. Hydrol. 324 (1–4), 10–23. http://dx.doi.org/10.1016/j.jhydrol.2005.09.008.

Vardavas, I., Chartzoulakis, K., Papamastorakis, D., Xepapadeas, A., Spanoudaki, K., Zacharioudakis, G., Kritsotakis, M., Bertaki, M., 2004. Report of Water Resources of Crete, 2004. Technical Report.

Wagener, T., Sivapalan, M., Troch, P.A., Woods, R.A., 2007. Catchment classification and hydrologic similarity. Geogr. Comp. 1 (4), 901–931.

Wang, X., Liang, Z., Wang, J., 2014. Simulation of runoff in Karst-influenced Lianjiang Watershed using the SWAT Model. Sci. J. Earth Sci. 4 (2), 85–92.

Wang, Y., Brubaker, K., 2014. Implementing a nonlinear groundwater module in the soil and water assessment tool (SWAT). Hydrol. Process. 28 (9), 3388–3403.

Ward, J.H., 1963. Hierarchical grouping to optimize an objective function. J. Am. Statist. Assoc. 58, 236–244.

Williams, P.W., 2004. Karst evaluation. In: Gunn, J. (Ed.), Encyclopedia of Caves and Karst Science, vol. 475. Fitzroy Dearbon, London, p. 8.

Wooldridge, S.A., Kalma, J.D., 2001. Regional-scale hydrological modelling using multiple-parameter landscape zones and a quasi-distributed water balance model. Hydrol. Earth Syst. Sci. Discuss. 5 (1), 59–74.

Yachtao, G.A., 2009. Modification of the SWAT Model to Simulate Hydrologic Processes in a Karst Influenced Watershed MS Thesis. Virginia-Tech, Department of Biosystems Engineering, Blacksburg.